A QUANTITATIVE ANALYSIS OF THE ATMOSPHERES OF THREE PECULIAR LOW-LUMINOSITY B STARS

Thesis by

John Charles Stewart

In Partial Fulfillment of the Requirements

for the Degree of

Doctor of Philosophy

California Institute of Technology

Pasadena, California

1955

ACKNOWLEDGMENTS

I wish to express here my sincere gratitude to Dr. Guido Münch, who suggested the problem, obtained some of the spectrograms, introduced me to the use of the 100-inch telescope and associated instruments, and whose generous advice and guidance during the entire investigation have been invaluable; to Dr. Jesse L. Greenstein, who supplied a number of fruitful suggestions and an unpublished line list for υ Sgr; to Dr. Donald E. Osterbrock, with whom I have had numerous discussions of various portions of the work; to my wife, Rachel W. Stewart, who assisted in the computations and in the drawing of the figures; to Dr. Lawrence H. Aller, of the University of Michigan, who made available unpublished equivalent-width measures for α Scl; and finally to the National Science Foundation, which by the award of a graduate fellowship supported the writer while this study was carried out.

ABSTRACT

High-dispersion spectra of HD 37058, HD 37129 and HD 135485, three B stars exhibiting spectral peculiarities, have been studied on the basis of model atmospheres, with a view to detecting abundance anomalies. An approximate theory of high-temperature model atmospheres, applicable to stars in the range of spectral type B1 - B7 and luminosity classes IV and V, has been developed and applied to the prediction of Balmer line profiles and total intensities of other lines. Temperatures, surface gravities and helium abundances of the three peculiar stars and two standard B stars, γ Peg and α Scl, have been determined. The abundances of other elements have been found from curves of growth using theoretical line strengths. The values of surface gravity derived imply luminosities lower than those of the standard stars. The helium abundance derived for HD 135485 is remarkably large; a sizable titanium excess and an oxygen deficiency were detected in HD 37058.

TABLE OF CONTENTS

CHAPTER I

Introduction

Among the stars of spectral type B, the fraction showing spectral peculiarities is somewhat smaller than in later types (1). As examples of peculiar B stars we may mention the Be stars and the B stars in the Pleiades, whose peculiarities may probably be interpreted as effects of axial rotation; and the helium-rich stars such as HD 124448, discovered by Popper, which exhibits a vanishingly small hydrogen abundance. Numerous investigations indicate, however, that among the ordinary B stars the hydrogen abundance is rather uniform (see, for example, the review article by Underhill (2)). Since energy considerations lead to ages for the brighter B stars which are shorter than the presently accepted time scale of the Galaxy, we should expect that if an evolving B star simply remained fixed in the H-R diagram and if mixing processes between atmosphere and interior were efficient enough, we would find a large range of values of the hydrogen abundance. We must, then, infer that before a B star is able to exhibit an appreciable change in its helium abundance it moves out of the B region of the H-R diagram. Popper's star might be interpreted as a star which was initially of another type, and which in the course of its evolution has moved into the B region.

It is the purpose of the present study to interpret the observed spectral peculiarities of three B stars in terms of the

physical conditions and chemical composition of their atmospheres, with special reference to the helium abundance. Some of these characteristics are evident at low dispersion and are the basis for the original classification of the stars as "peculiar". Others show up in a visual inspection of high-dispersion plates, while microphotometer tracings are necessary to find quantities such as the extent of the wings of the hydrogen lines.

The three stars chosen for study are HD 135485, a sharp-lined object well above the galactic plane; HD 37058, a sharp-lined member of the Orion aggregate; and HD 37129, similar to HD 37058 but apparently rotating. The pertinent information concerning these stars follows (3-6):

	HD 135485	HD 37058	HD 37129
Spectral type			
Mt. W. R. V. Cat.	cB5	B3	B3
Yerkes (Sharpless)		B2Vp	B2Vp
Victoria	B3sk	B3sk	
m_{visual}	8.3	7.3	7.0
R. V. (km/sec)	-12	+23	+28

The reported peculiarities at low dispersion are the sharpness of the metallic lines of HD 135485, which undoubtedly was

the basis for the "supergiant" classification, and the apparent weakness of the helium lines in HD 37058 and HD 37129, mentioned by Sharpless. The description of the high-dispersion characteristics will be deferred until mention has been made of the data obtained for this study.

Bearing in mind the desirability of differential as well as absolute analyses, two standard stars were chosen, of spectral types approximating those of the peculiar stars: γ Peg (B2.5 IV) and α Scl (B5 V), both of which are sharp-lined stars. γ Peg has been the subject of analyses by Aller (7) and Neven (8); α Scl is part of an as yet unpublished investigation by Aller.

Observational Material

All of the observational material used in this study was obtained with the coudé spectrograph of the 100-inch Hooker telescope on Mt. Wilson. The 32" camera and 15,000 lines/inch grating were used, giving a dispersion of 10.2 Å/mm in the second order. The spectra were widened by trailing in right ascension. All plates were taken on Eastman IIa-O emulsion, baked before exposure for 72 hours at 50° C. to increase the effective speed, and developed in D-19 using a mechanical tray rocker. Exposure times were on the order of two hours.

Strip-calibration spectra flanking the stellar spectra were exposed concurrently with the latter; exposure times were chosen roughly equal to the total intermittent stellar exposure caused by trailing.

Tracings at a magnification of about 200 were made with a transmission-type microphotometer. Profiles of the strong lines were reduced to intensity point by point; weak lines were approximated by triangles.

Wavelength measures were made using iron-arc comparison spectra; for HD 37058 these were supplemented by measures directly from the tracing, since a good many lines clearly visible on the tracing were invisible under the measuring microscope. The tracing measures, using well-established stellar lines as standards,

appeared to give less scatter with respect to the laboratory wavelengths, particularly for the H and He lines (as expected) but also for sharp and weak lines.

Identifications were made chiefly from the RMT (9), but also from published work of Struve (10) and Aller (7) and an unpublished line list of Greenstein for υ Sgr. Four lines at λ 4200 in HD 37058 were tentatively identified as Ti III from the original analysis of this spectrum by Russell and Lang (11).

The wavelengths, equivalent widths, and identifications are presented in the Appendix. For HD 135485 the values given are means for three plates; for HD 37058 the wavelengths are the mean, when available, of tracing and microscope measures; and for HD 37129 the wavelengths are only rudimentary, since only strong well-known lines appear at all. Some identifications--particularly contributors to blends--have been revised as a result of the curve-of-growth analyses made later. Parenthetical identifications denote minor contributors to blends, poor wavelength agreement, or general implausibility.

Equivalent widths of the H lines and of lines strongly blended with them are omitted; Balmer profiles are given separately. Ca II H and K are omitted since they are evidently of interstellar origin. An intercomparison of the three plates of HD 135485 yielded an estimate of 20% for the probable error of the equivalent width of a

weak line.

The plates used are as follows:

Star	Plate	Observer	Date	Spectrum width (mm)	Remarks
HD 135485	Ce 8680	Münch	3/25/53	0.4	Slightly under-exposed
"	Ce 9294	"	6/19/54	0.4	
"	Ce 9330	"		0.4	Fog at λ<4100
HD 37058	Ce9572	Stewart	12/17/54	0.8	
"	Ce 9605	"	1/8/55	0.4	Intentionally overexposed. Used only for λ's in UV.
HD 37129	Ce 9583	"	12/19/54	0.8	
α Scl	Ce 9386	Münch	9/9/54	0.4	Used for H profiles only.

Comparison Stars

Measures of equivalent widths of the He and Si lines and the profile of Hδ were taken from Aller's analysis of the atmosphere of γ Pegasi (7). These measures are based on McDonald and Victoria prism plates, and Mount Wilson grating plates corrected for scattered light. Since the measures on the three peculiar stars were not corrected, I have removed Aller's correction so as to place the two sets of measures on the same system. This amounts to a reduction of all Aller's line depths and equivalent widths by .10 in the logarithm. For α Sculptoris the He and relevant Si equivalent widths were taken from unpublished measures by Aller on a Mount Wilson coudé plate. The values of W follow:

Elem.	λ	W(mÅ)	Elem.	λ	W(mÅ)
He I	4471	275	Si III	4575	29
	4438	41		4568	27
	4388	217		4552	50
	4144	130			
	4121	71	Si II	4131	94
	4026	528		4128	81
	4009	119			
	3965	36			
	3867	44			
	3819	499			

Qualitative discussion of high-dispersion data

The spectra of the two stars in the Orion aggregate, HD 37058 and HD 37129, are so similar in all respects except line sharpness as to suggest that they would appear identical if they had the same rotational velocity. The profiles and intensities of the H and He lines are essentially the same; lines of other elements are in general measured slightly stronger in HD 37058 than in HD 37129, but this may be a spectrophotometric effect (Eberhard effect and/or finite analyzing slit width). Line ratios (in particular, Si III/Si II) are the same in the two stars. Accordingly, when reference is made to HD 37058 in what follows, and the property referred to is observable in both stars, HD 37129 is included by implication.

The Si III/Si II and Fe III/Fe II line ratios define a sequence of decreasing ionization: γ Peg, HD 37058, α Scl, HD 135485. Since the widths of the H lines do not differ greatly, the range of electron pressures is not large and the ionization sequence must be the correct temperature sequence. Conclusions drawn from peculiarities observed at low dispersion may be misleading; the extended wings of the H lines in the "supergiant" HD 135485 and the appearance of the forbidden He I line at λ 4470 place this star on or near the main sequence. The "weakness" of the He lines in HD 37058 estimated by Sharpless is not confirmed by the measures either, for the total intensities are at least as large as in γ Peg.

However, the wings of the lines, more extensive than in γ Peg, could easily be invisible at low dispersion.

The most striking feature in the spectrum of HD 135485 is the great strength of the He lines; indeed, they are stronger than in any other star in this study, though this is the coolest star. In the main sequence (12) the He lines reach maximum strength around spectral type B2 and decrease fairly rapidly with decreasing temperature, so a normal star of the same level of ionization as HD 135485 would show weaker He lines than α Scl. No explanation save that of a high He abundance seems plausible.

High He abundance has been suggested as a characteristic of Population II stars. It would therefore be interesting to determine whether HD 135485 satisfies other Population II criteria. The galactic coordinates ($l = 316^{\circ}$, $b = +34^{\circ}$) place it about 450 psc above the galactic plane and 700 psc toward the galactic center if the absolute magnitude is taken (13) as -1.3; this height is rather large for a Population I B star but not implausibly so. The absolute magnitude, however, is merely a guess. The radial velocity is low. Thus HD 135485 cannot be assigned on dynamical grounds to either population type.

Turning now to HD 37058, we find that Ti II shows about the same strength as in α Scl, while Fe II is considerably weaker. Neither ion appears at all in γ Peg. This indicates an excess of

Ti relative to Fe in HD 37058, which is confirmed by a consideration of Ti III. The second and third ionization potentials of Fe and Ti are such that Fe III and Ti III are the predominant stage of ionization in stars of this type; Fe III has about the same strength in HD 37058 as in γ Peg. Hence any sizable difference in the strength of Ti III must reflect either an excitation effect or an abundance effect. Russell and Lang (11) list four lines of Ti III in the observable region:

λ	Int.
4215.55	5
4207.54	3
4204.95	2
4200.11	2

All of these appear in HD 37058 with good wavelength agreement and in the proper intensity sequence except for the last, which is blended with a line of Fe III. For the other three no other plausible identification is found; the most likely candidate, Cr II, fails to show the other lines in its multiplets. The resonance line λ 4215.52 of Sr II could account for part of the strength of the observed λ 4215.6 line; but the other resonance line λ 4077.7, if indeed present, is too weak to admit Sr II as the sole contributor to λ 4215.6.

In Aller's list for γ Peg the only near wavelength coincidence with the Ti III lines is λ 4199.95, attributed to A II,

with W = 23 mÅ. This line also appears in the very complete list by Underhill (14), with intensity O. At the wavelengths of the Ti III lines in the same list, nothing stronger than 00 appears. Thus it is evident that the Ti III lines are weaker in γ Peg by a fairly considerable factor, and since an excitation effect would operate in the opposite sense a genuine abundance difference is indicated.

Another qualitative difference between HD 37058 and γ Peg is the relative weakness of the O II lines in HD 37058. Since these lines originate in levels of high excitation potential, however, their treatment will be left to the quantitative portion of this study, to which we now proceed.

CHAPTER II

Method of Analysis

The ultimate goal of the theory of stellar atmospheres is the prediction of the complete observable spectrum from given values of the surface gravity, integrated emergent flux of radiation, and atmospheric chemical composition of a star. These parameters are in principle sufficient, in the case of an atmosphere whose geometrical height is small compared to the radius of the star and which is spherically symmetrical, for the prediction of the emergent monochromatic flux at all wavelengths. In the case of B stars the problem may conveniently be split up into three parts: (A) Structure of the atmosphere (i.e., temperature as a function of electron pressure); (B) the resulting flux in the continuum and in the lines of hydrogen and helium; and (C) the flux in the lines of other elements. These parts can be treated successively, with only (C) depending on abundances of elements heavier than He, under the following approximations:

(1) The continuous absorption coefficient due to elements other than H and He is negligible.

(2) Nearly all of the free electrons result from the ionization of H and He.

(3) The total flux removed by lines of elements other than H and He is negligible compared to the total emergent flux.

These approximations are very well satisfied in B stars (though all of them fail in cool types). For the treatment of parts (A) and (B), then, only three parameters are necessary, which may be taken as the surface gravity g, boundary temperature T_o, and helium abundance (by mass) Y. Part (C) depends also on the abundances of other elements.

Rough values of g, T, and abundances are frequently gotten by assuming an isothermal atmosphere at constant pressure, but for more precise work a model atmosphere is mandatory. When the continuous absorption coefficient varies with frequency as strongly as it does in B stars, however, the usual "grey-atmosphere" solution, formed by replacing the actual absorption coefficient k_ν by some "mean" value k independent of frequency, is only a first approximation. The question of what mean to use is to some extent arbitrary and has been discussed by Michard (15). He finds that the condition of constant total flux is best satisfied by the Planck mean ($k_{Pl} = \int_o^\infty k_\nu \frac{B_\nu}{B} d\nu$) but that the value of the total flux differs from that of the equivalent grey atmosphere (which has the same temperature distribution with pressure); that is, the ratio of the boundary and effective temperatures is changed. This is in accord with numerical work by Pecker (16), McDonald (17), and Underhill (18), all of whom found a larger ratio of effective to boundary temperature than holds for a grey atmosphere. The use

of the Rosseland mean attempts to force a fit between the grey and non-grey fluxes, and in the process loses constancy of flux with depth. Michard made numerical applications to the relatively mildly non-grey case of the sun. It is worth noting that the Planck mean and the Chandrasekhar mean are very nearly the same numerically but the Planck mean is much more convenient to use. It may be tabulated, like the Rosseland mean, as a function of temperature and pressure once and for all, while the Chandrasekhar mean must be computed anew for each boundary temperature.

Since in this investigation the effective temperature, as such, will not enter, there is no advantage to be gained by demanding the grey-atmosphere ratio of boundary and effective temperatures. Accordingly the Planck mean has been used throughout, except in one model which was constructed with the Chandrasekhar mean to check some approximations, and the models are characterized by T_o. Following the usual practice, the opacity integral has been cut off at the Lyman limit. The contribution of helium to the total opacity has been taken into account in an approximate fashion, and the contributions of electron scattering and H^- have been neglected.

With model atmospheres available for a range of T_o, g, and Y, the observational data may be fitted by a properly chosen model. Neven (8) has fitted models to the observed Balmer discontinuity and number of H lines; ''ler (7) used the profile of H δ .

In both cases adjustments had to be made to account for the central intensities of the H lines. Neven assumed pure absorption and modified the T (τ) distribution in the outermost layers, while Aller kept T (τ) fixed and introduced scattering in the proper amount. It is difficult to see how both temperature and gravity can be determined by the latter procedure; Aller states that a lower temperature and lower gravity would also fit, but rejects the lower values on mass-luminosity grounds. Thus he essentially uses the wings of the line to determine a relation between T and g, and then guesses g. I have preferred to assume pure absorption and not to expect to fit the core of the line, since here both theory and observation have large uncertainties. The wings of the H lines are relatively sensitive to g and insensitive to T_o; as a quantity sensitive to T_o the ratio of the equivalent widths of two lines of some other element, separated by a large range of excitation potential, would be suitable. I have chosen the 4560 multiplet of Si III and the 4130 multiplet of Si II, which have a total energy separation of 25 ev. Since these lines come from two stages of ionization the electron pressure enters, and a second relation between T_o and g is gotten. Both relations depend very slightly on Y, and not at all on the Si abundance. A third relation connects T_o, g, and Y through the total equivalent widths of wide and shallow He lines. The three relations can then be solved for the three parameters. To evaluate the

theoretical equivalent widths of the Si and He lines the method of weighting functions was used, with saturation of the Si lines taken into account approximately by the use of a Milne-Eddington curve of growth. The method amounts to evaluating a weighted mean value of η and entering the curve of growth with this. Thus the principal parts, at least, of both stratification and saturation effects are eliminated. For the He lines used saturation is neglected because of the great Stark width.

With T_o, g, and Y determined, the abundances of elements for which absolute f-values or theoretical line strengths are available can be derived. Absolute LS coupling line strengths in the Coulomb approximation have been computed for the observed lines of the lighter elements, using the tables of Bates and Damgaard (19); intermediate-coupling strengths for a number of O II lines have been taken from the computations of Garstang (20). Using these strengths, the abundances of the light elements have been obtained by the use of the conventional Milne-Eddington curve of growth.

Absolute Line Strengths

For the determination of stellar abundances of the elements it is necessary to have absolute f-values or theoretical strengths for the observed transitions unless one is content with relative abundances from star to star. In the Russell-Saunders (LS) coupling scheme the strengths of lines in a whole transition array are readily found in terms of a constant factor characteristic of the array (21). This factor (in atomic units) is

$$\sigma^2 = \frac{1}{4l^2 - 1} \left[\int_0^\infty r\, R(n,1)\, R(n,\, l-1)\, dr \right]^2$$

where the R's are radial eigenfunctions of the jumping electron in the two configurations. On the basis of the Coulomb approximation, Bates and Damgaard (19) have computed tables from which σ^2 can be found from the term values of the levels involved. The general formulae for strengths of multiplets in an array and of lines in a multiplet are conveniently presented, by Goldberg (22) and White and Eliason (23) respectively, in the form of tables.

Using the above sources, absolute strengths S in atomic units ($a_o^2\, e^2$) were computed for observed lines of those elements whose line spectra were reasonably well represented. Fe II and Ti II were omitted since the work of Wright (24) and others indicates that LS coupling is a poor approximation for these complex atoms;

f-values for H and He I are published. In general σ^2 was computed using term values from each observed multiplet, and a mean of the resulting values of σ^2 was adopted for the array. The scatter in σ^2 was of the order of 10% or less.

Nearly all the observed lines of elements other than Fe and Ti appear to follow LS selection rules; a notable exception is a strong multiplet of Si II at λ 3860 which is a two-electron jump.

S rather than f is tabulated for reasons of convenience. The values of S given here may be converted to f-values by using the standard relation

$$\lambda gf = 304\ S$$

where g = statistical weight of lower level, and λ is in Ångstroms. Table 4 lists the radial-integral factor σ^2, while Table 5 gives the absolute multiplet strengths S(M) and line strengths S. Primes on the array designation denote an elevated parent term, explicitly given in Table 4 (closed subshells are suppressed). Excitation potentials are mean values for the lower term.

Garstang (20) has computed line strengths for certain transition arrays of O II and S II, in the intermediate-coupling (IC) scheme. This approximation includes the effects of spin-orbit interactions, but not configuration interactions. These are listed as S(IC) and are used in the analysis, when available, rather than LS strengths.

Numerical model atmosphere

In order to check the validity of one or two approximations (in particular the neglect of electron scattering) a model atmosphere intended to represent a main-sequence star of about spectral type B3 or B4 was constructed by conventional methods. The assumed parameters were $Y = 0$ (pure hydrogen), $T_o = 15,000^o$, and $\log g = 4.10$. The Gaunt factors for hydrogen were roughly included in forming the absorption coefficient, and the Chandrasekhar-mean opacity was used, truncated at the Lyman limit. The exact grey-body temperature distribution by Mark (25) was assumed. The electron pressure was set equal to one-half the gas pressure throughout. Then the equation of hydrostatic equilibrium takes the form

$$\frac{dP_e}{d\tau} = \frac{g/2}{P_e K(\tau) + \sigma}$$

where

$K(\tau)$ = opacity computed at depth τ, per unit electron pressure

σ = electron scattering cross section (per gram of stellar material) $= .404\ cm^2/gm$

Initially σ was neglected and the resulting equation

$P_e^2 = g \int_0^\tau \frac{d\tau}{K(\tau)}$ was integrated; then σ was inserted

and iteration led to the final model. The initial and final models are exhibited in Table 1.

The influence of electron scattering is seen to be small; the change in P_e due to its inclusion is less than 5% at $\tau \approx 2/3$. A somewhat larger change would be expected if the hydrogen abundance were lower, as helium has a smaller absorption coefficient per unit mass. If the helium opacity is considered as hydrogenlike, i.e., if $K(\tau)$ is simply reduced by a constant factor, then it is clear that an increase in g by the same factor will give a new model whose electron pressure is a constant multiple of the old and in which electron scattering is the same fraction of the opacity. In a qualitative way it can be seen that a higher temperature, lower surface gravity or higher helium abundance will increase the relative importance of electron scattering.

The model was tested for convection using Schwarzschild's criterion. The temperature gradient is about one-half the adiabatic gradient at $\tau = 3$ and is less for smaller τ, indicating no convection in observable layers. This test is perhaps trivial, since no partially-ionized component of the stellar material has been included. One would expect convection to occur, for example, in helium-rich stars of about type B5, where helium is just becoming ionized in the atmosphere.

The importance of radiation pressure in the structure of

the atmosphere was roughly evaluated. Allowing for this entails the replacement of g by g-g′ where $g' = k(\tau)\sigma_R T_e^4/c$ and varies through the atmosphere. At $\tau = .50$, g′ is around one-tenth of g, so its inclusion would change P_e by about 5% in the same direction as the inclusion of electron scattering. At small τ, g′ is negligible.

TABLE I

NUMERICAL MODEL ATMOSPHERE

		Initial		Final	
τ	T	$\log P_e$	$P_e K(\tau)$	$\log P_e$	$P_e K(\tau)$
0	15,000	$-\infty$	0	$-\infty$	0
.01	15,110	1.93	1.45	1.82	1.11
.05	15,540	2.29	2.92	2.24	2.62
.10	15,900	2.46	3.76	2.42	3.46
.20	16,530	2.64	4.62	2.61	4.36
.30	17,050	2.76	5.19	2.73	4.88
.40	17,540	2.84	5.40	2.81	5.17
.50	17,990	2.90	5.69	2.88	5.38
.60	18,350	2.96	5.75	2.94	5.49
.70	18,690	3.01	5.75	2.99	5.57
.80	19,080	3.05	5.75	3.03	5.56
.90	19,400	3.09	5.75	3.07	5.55
1.00	19,700	3.13	5.75	3.11	5.51
1.20	20,250	3.19	5.69	3.18	5.42
1.40	20,780	3.25	5.56	3.24	5.34
1.60	21,250	3.30	5.44	3.29	5.30
1.80	21,700	3.35	5.40	3.34	5.27
2.00	22,150	3.39	5.37	3.38	5.21
2.50	23,100	3.48	5.30	3.47	5.12
3.00	23,950	3.56	5.19	3.55	5.02

CHAPTER III

Evaluation of the Planck mean opacity for hydrogen:

By definition $k_{Pl}(T) = \int_0^\infty k'_\nu(T) \frac{B_\nu(T)}{B(T)} d\nu$

where $k'_\nu(T)$ = monochromatic continuous absorption coefficient at frequency ν, corrected for induced emission,

$B_\nu(T)$ = monochromatic Planck function =

$$\frac{2h}{c^2} \frac{\nu^3}{e^{h\nu/kT} - 1},$$

$$B(T) = \int_0^\infty B_\nu(T)\, d\nu .$$

In applying this formula to the case of B stars it must be kept in mind that the integral, as it stands above, is dominated by the contribution from the Lyman continuum, whereas most of the flux passes to the red of the Lyman limit. "Ideally" the weighting function should be the flux rather than B_ν, and the procedure used in the case of the Chandrasekhar mean should be valid also for the Planck mean--i.e., the integral is cut off at the Lyman limit. Then

$$k = \frac{\int_0^{\nu_1} k'_\nu B_\nu\, d\nu}{\int_0^{\nu_1} B_\nu\, d\nu}$$

where ν_1 is the frequency at the Lyman limit.

It is convenient to rewrite this in terms of $u \left(= \frac{h\nu}{kT} \right)$ and to divide numerator and denominator by B(T). Then since at constant

T

$$\frac{B_\nu \, d\nu}{B} = \frac{15}{\pi^4} \quad \frac{u^3 \, du}{e^u - 1} \quad ,$$

we have

$$\int_0^{\nu_1} k'_\nu \, \frac{B_\nu}{B} \, d\nu = \frac{15}{\pi^4} \int_0^{u_1} k'_u \quad \frac{u^3 \, du}{e^u - 1}$$

and

$$\int_0^{\nu_1} \frac{B_\nu}{B} \, d\nu = \frac{15}{\pi^4} \int_0^{u_1} \frac{u^3 \, du}{e^u - 1} \quad .$$

Let us first consider the first integral, the numerator of k.

$k'_u = k_u (1 - e^{-u})$ where k_u = absorption coefficient uncorrected for induced emission

so

$$\int_0^{u_1} k'_u \quad \frac{u^3 \, du}{e^u - 1} = \int_0^{u_1} k_u \; u^3 \; e^{-u} \; du \quad .$$

In the case of hydrogen, neglecting Gaunt factors and line absorption but including free-free transitions, the absorption coefficient for $\nu_i > \nu > \nu_{i+1}$ is (26)

$$k_i(u, T) = C\ (\nu_1/\nu)^3 \left\{ \sum_{\nu_n < \nu}^{\infty} \frac{1}{n^3}\, e^{-(u_1 - u_n)} + \frac{e^{-u_1}}{2u_1} \right\}$$

where

$$\nu_i = \frac{\nu_1}{i^2} \quad ; \quad u_i = \frac{u_1}{i^2} \quad ; \quad u_1 = \frac{h\nu_1}{kT}$$

$$C = 4.74 \times 10^6 \text{ cm}^2 \text{ per gm of H in state } n = 1.$$

This may be written as

$$k_i(u, T) = \frac{1}{u^3} f_i(T),$$

with

$$f_i(T) = C' T^{-3} e^{-u_1} \left\{ \sum_{n=i+1}^{\infty} \frac{1}{n^3} e^{u_n} + \frac{1}{2u_1} \right\}$$

and

$$C' = C u_1^3 T^3 = C \left(\frac{h\nu_1}{k} \right)^3 .$$

Now the contribution of the region from u_i to u_{i+1} to the integral over u is just

$$\int_{u_{i+1}}^{u_i} k_i(u, T)\, u^3\, e^{-u}\, du = \int_{u_{i+1}}^{u_i} f_i(T)\, e^{-u}\, du = f_i(T) \left\{ e^{-u_{i+1}} - e^{-u_i} \right\}$$

and these contributions are to be summed over the range of i

desired. To cut off the Lyman continuum one takes i = 1 to ∞, so that

$$\int_0^{u_1} k_\nu(u,T)\, u^3\, e^{-u}\, du = \sum_{i=1}^{\infty} f_i(T) \left\{ e^{-u_{i+1}} - e^{-u_i} \right\} =$$

$$= f_1(T) \left\{ e^{-u_2} - e^{-u_1} \right\} + f_2(T) \left\{ e^{-u_3} - e^{-u_2} \right\} + \cdots$$

$$= - f_1\, e^{-u_1} + e^{-u_2}(f_1 - f_2) + e^{-u_3}(f_2 - f_3) + \cdots$$

$$= - f_1\, e^{-u_1} + \sum_{i=2}^{\infty} e^{-u_i} (f_{i-1} - f_i) \ .$$

Now note that $f_{i-1} - f_i = C' T^{-3} e^{-u_1} \left\{ \frac{e^{u_i}}{i^3} \right\}$

so

$$\int_0^{u_1} k_\nu(u,T)\, u^3\, e^{-u}\, du = C' T^{-3} e^{-u_1} \left[\sum_{n=2}^{\infty} \frac{1}{n^3}\, e^{u_n - u_1} - \frac{e^{-u_1}}{2u_1} + \sum_{n=2}^{\infty} \frac{1}{n^3} \right]$$

$$= C' T^{-3} e^{-u_1} \left[\sum_{n=2}^{\infty} \frac{1}{n^3} \left(1 - e^{u_n - u_1}\right) - \frac{e^{-u_1}}{2u_1} \right] .$$

For temperatures under 30,000° this expression simplifies considerably, since then $u_1 = 13.60 \ \frac{11,600}{T} > 5$ and $u_1 - u_n > 3.9$; to within better than 2% all terms in the brackets may be neglected except $\sum_{n=2}^{\infty} \frac{1}{n^3}$ (= .202) and we then have

$$\int_0^{\nu_1} k'_\nu \frac{B_\nu}{B} \, d\nu = \frac{15}{\pi^4} (.202) C' T^{-3} e^{-u_1}.$$

Now consider the other ("normalizing") integral, $\int_0^{\nu_1} \frac{B_\nu}{B} \, d\nu$. This will be close to unity except at very high temperatures, since it represents the fraction of the blackbody energy curve which lies to the red of 912 Å. It is given by $\frac{15}{\pi^4} \cdot \int_0^{u_1} \frac{u^3 \, du}{e^u - 1}$ and is easily evaluated for $u_1 > 5$. (For smaller u_1 -- i.e., higher temperature--Rudkjøbing (27) has computed the integral from u_1 to ∞ by numerical integration.) The reciprocal of this integral will be denoted by N(T) and is tabulated; however, since $N(T) < 1.05$ for $T < 20,000^\circ$, in most applications N(T) will simply be set equal to unity.

We can now write the opacity as

$$k = \frac{15}{\pi^4} (.202) C' T^{-3} e^{-u_1} N(T) \text{ cm}^2 \text{ per gm of H in n = 1.}$$

For the range of temperature and electron pressure encountered in B stars, hydrogen is nearly all ionized and it will be more convenient to refer the opacity to a gram of H ions. The Saha equation gives the required ratio:

$$\frac{\text{H I (n = 1)}}{\text{H II}} = 10^{0.48} P_e T^{-5/2} e^{u_1}$$

and upon inserting all the constants

$$k = 1.75 \times 10^{21} P_e T^{-11/2} N(T) \text{ cm}^2 \text{ per gm of } H^+$$

or

$$k = 7.61 P_e \theta^{11/2} N(\theta)$$

for pure hydrogen.

Approximate helium opacity

In this investigation it is suspected that anomalous helium abundances may be encountered. For this reason it is desirable to have some way of adjusting the contribution of He to the total opacity without undue labor. Frequently the helium abundance is guessed at the start in order to compute the opacity, and revision of the whole computation becomes necessary to reconcile the assumed and observed abundances. It will be seen that with a couple of plausible approximations, the helium abundance can be carried through as a free parameter until it is evaluated using the He lines. These approximations are:

(1) All levels of He I (except the ground level) of principal quantum number n lie as far below the ionization limit as does the nth state of hydrogen.

(2) Absorption cross sections (per atom) of all levels (except the ground level) are hydrogenlike.

The ground level is exempt because the absorption limit from this

state lies at 504 Å, beyond the Lyman limit; unless the temperature is extremely high and/or the hydrogen abundance nearly zero, the flux here will be very small and the opacity integral can be cut off at the Lyman limit.

An inspection of the He I absorption cross sections computed by Huang (28) and Goldberg (29) shows that the weighted mean of the $2\,^1P$ and $2\,^3P$ cross sections is, indeed, close to the value for hydrogen in ($n = 2$), while $2\,^1S$ and $2\,^3S$ depart in the sense of a smaller cross section and shorter limiting wavelength. The departures are not large, however, and are partially compensated for by the increase in population resulting from the Boltzmann factor; furthermore the weight of the 2S states in forming a "mean $n = 2$ state" for He I is only 1/3 the weight of the 2P states.

It is therefore evident that the above approximations will have only a very small influence on the total opacity. Their use in forming the monochromatic absorption coefficient is not as safe; but all the lines to be used in the analysis lie in the wavelength range λλ3700 - 4900, where k_ν is determined only by the very nearly hydrogenlike states $n = 3, 4, 5, ..,$ so the approximations should be more than adequate.

To arrive at the opacity per gram of ionized He, then, it is only necessary to use the Saha equation to relate the number of atoms in the nth state to the number of ions. Since $g_n = 4n^2$ and

$g_{ion} = 2$ for He, and $g_n = 2n^2$ and $g_{ion} = 1$ for H, this ratio is exactly the same as for H, so the opacity of He per He ion equals the opacity of H per H ion. The difference in atomic mass and the possibility of incomplete ionization of helium yields finally for the opacity of a mixture of H and He:

$$k = 1.75 \times 10^{21} \, (X + (1/4)Yy) \, P_e \, T^{-11/2} \, N(T)$$

where X = abundance of H by mass

Y = abundance of He by mass

$y = \frac{\text{He II}}{\text{He (total)}}$

and the hydrogen has been taken as mostly ionized.

Other sources of opacity

While neutral hydrogen and helium are clearly the chief contributors to the opacity in the relevant range of T and P_e, other sources must be examined to see whether they contribute appreciably. Possible suspects are singly ionized helium, negative hydrogen ions, and free electrons. Very rough considerations are sufficient to eliminate the first two; electron scattering was included in the numerically-integrated model, where it was dominant only in the extreme outermost layers ($\tau < .002$) but contributed about 7% of the total opacity through the layers with $\tau > .1$. Its neglect will cause an error of this order in the deduced surface gravity (where

an uncertainty of 50% is rather good) but its influence on the monochromatic absorption coefficient may be somewhat larger in transparent regions of the spectrum. In a giant or supergiant B star it would certainly not be permissible to neglect electron scattering, but in dealing with the present low-luminosity objects it will be omitted in the analysis and compared as a check with the opacity of the final models.

Comparison with other opacities

It is of interest to compare the numerical values of the Planck mean opacity (k_{Pl}) with the values of the Chandrasekhar and Rosseland opacities (k_{Ch}, k_R). The values of k_{Ch} used in the construction of the numerical model, per gram of H^+ and per unit electron pressure, are shown in Fig. 1 together with k_{Pl} and k_R for the same temperature, the latter being taken from Unsöld (26). The close agreement between k_{Pl} and k_{Ch}, predicted by Michard (15) and demonstrated by him for the sun, is here seen to hold even for the more severe variations of k_λ found in B stars. Even the slight tendency of k_{Ch} to fall below k_{Pl} may perhaps be ascribed to the Gaunt factors neglected in forming the latter.

The large factor by which k_R differs from the other two suggests how a part, at least, of the well-known discrepancy between spectroscopic and dynamical surface gravities may arise. Consider

two models having the same structure $T(P_e)$ and therefore the same spectrum. Suppose that both were constructed using the grey-atmosphere temperature distribution $T(\tau)$ but that the opacities used differed by a constant factor. Then since $\frac{dP_e}{d\tau}$ is the same in the two models, the equation of hydrostatic equilibrium requires that

$$g_1/k_1 = g_2/k_2$$

and the spectroscopically deduced surface gravity depends directly on the choice of k. Evidently in the B-star temperature range the use of k_R instead of k_{Pl} or k_{Ch} can reduce the deduced surface gravity by a factor as large as 3.

FIGURE 1
HYDROGEN OPACITIES

LOG k IN cm^2/gm OF H^+ PER UNIT ELECTRON PRESSURE

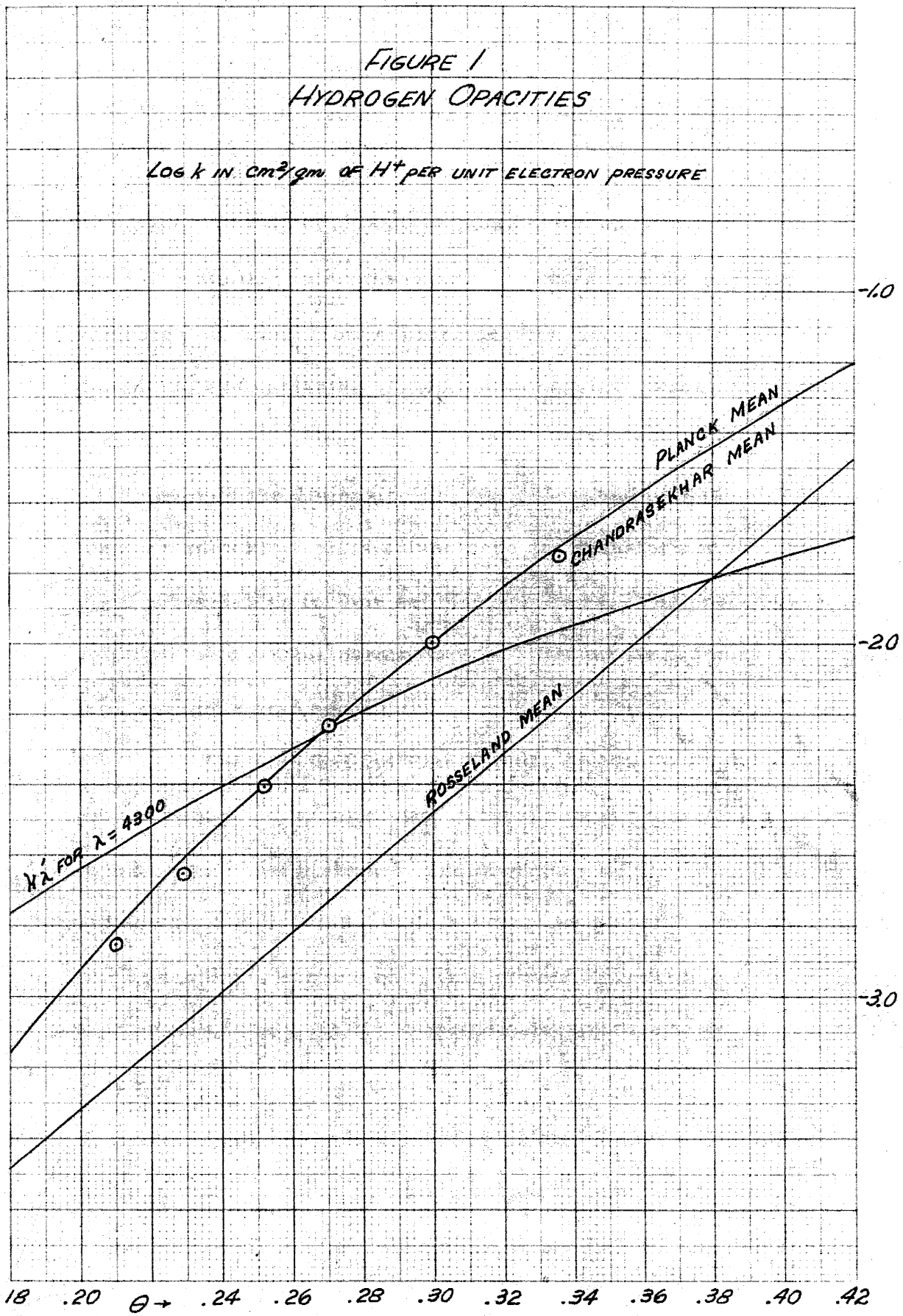

CHAPTER IV

Homology-invariant model atmospheres

In the theory of stellar interiors the approximation of the opacity and energy production by power laws in the density and temperature leads to homology-invariant models for the stellar interior. By this is meant that if one expresses the physical variables (distance from center, density, temperature) in terms of dimensionless variables multiplied by physical parameters (radius, central density, central temperature), the problem reduces to one involving only the dimensionless variables (and perhaps a dimensionless parameter) which is solved once and transformed back into physical variables for any set of parameters. The process yields relations between the parameters of different stars (mass-luminosity law, energy-output equation).

The fact that the Planck mean opacity for hydrogen and helium reduces to a power law in the electron pressure and temperature suggests that a similar treatment may be possible for model atmospheres constructed with this opacity law, if the gas pressure can be similarly expressed. This proves to be true in general. It also proves to be possible to include electron scattering (treated as absorption) if a dimensionless parameter is introduced. The equations for these general cases will be displayed, but the actual solution will be confined to the relevant case of negligible electron scattering, with gas pressure equal to a constant times electron

pressure.

(I). We start with the equation of hydrostatic equilibrium:

$$\frac{dP_g}{d\tau} = \frac{g}{k}$$

and the temperature distribution with optical depth:

$$T^4/T_o^4 = \frac{\tau + q(\tau)}{q(o)}$$ (known from the solution of the transfer problem)

where P_g = gas pressure

g = surface acceleration of gravity

k = Planck mean opacity

τ = mean optical depth

T_o = boundary temperature

Introducing dimensionless variables

$$t = T/T_o \qquad p = P_e/P_o$$

where P_o is a free parameter for the present, and letting

$$P_g = P_g(P_o, T_o)\, p^a\, t^b$$
$$k = k(P_o, T_o)\, p^c\, t^d$$

we get

$$P_g(P_o, T_o)\, k(P_o, T_o)\, p^c\, t^d\, d(p^a\, t^b) = g\, d\tau$$

or
$$\left[\frac{P_g(P_o, T_o)\, k(P_o, T_o)}{g}\right] p^c\, t^d\, d(p^a\, t^b) = d\tau$$

Now by an appropriate choice of P_o the (dimensionless) quantity in brackets may be made equal to any convenient constant, say unity, and we are left with a differential equation in p and t after eliminating τ by the use of

$$t^4 = \frac{\tau + q(\tau)}{q(o)}$$

The equation is to be solved under the boundary condition $t = 1$ when $p = o$.

(II). A slightly different procedure allows the inclusion of a constant contribution to the opacity. Restricting ourselves for brevity to the case

$$P_g = 2\, P_e\,, \qquad k = C P_e T^{-11/2} + \sigma$$

$$T^4/T_o^4 = 1 + 3/2\ \tau$$

and making, as before, the substitutions

$$t = T/T_o\,, \qquad p = P_e/P_o$$

where P_o is again free, there results

$$(CP_o T_o^{-11/2}\, p\, t^{-11/2} + \sigma)\, 2\, P_o\, dp = \frac{2}{3}\, g\, d\,(t^4).$$

Choosing $P_o = \sigma\, T_o^{11/2}/C$,

$$(p + t^{11/2})\, \frac{3\sigma P_o}{4\, g}\, dp = t^{17/2}$$

or $$A\, \frac{dp}{dt} = \frac{t^{17/2}}{p + t^{11/2}}$$

which contains the single dimensionless parameter $A = \dfrac{3\sigma^2\, T_o^{11/2}}{4\, g\, C}$, and is subject to the boundary condition $t = 1,\ p = 0$.

This equation is rather intractable and its numerical solution for several values of A scarcely seems worthwhile. It will therefore be relegated to the status of an amusing relation, possibly useful in the construction of supergiants.

(III). The case of interest is the special case of (I) in which

$$a = 1,\quad b = 0,\quad c = 1,\quad d = -\frac{11}{2}$$

$$P_g\,(P_o, T_o) = C_1 P_o$$

$$k\,(P_o, T_o) = C_2 P_o T_o^{-11/2}$$

and instead of using the exact $q\,(\tau)$ of Mark, we will adopt the classical approximation $q\,(\tau) = 2/3$. Omitting the algebra, the result is

$$p^2 + 1 = t^{19/2}$$

where P_o has been chosen so that

$$P_o^2 = \frac{32}{57} \quad \frac{g\, T_o^{11/2}}{C_1 C_2} \quad .$$

From the derivation of the Planck mean we got $C_2 = 1.75 \times 10^{21} \cdot (X + \frac{1}{4} Yy)$, and for a mixture of ionized H and partly-ionized He the relation between gas and electron pressures is

$$P_g/P_e = 2\,(X + \tfrac{1}{8} Y(1 + y))/(X + \tfrac{1}{4} Yy) = C_1.$$

If the range of T and P_e of a given model is such that y changes appreciably through the atmosphere, the above treatment is not strictly valid, and y must be interpreted as some mean value.

Letting $Q = X + \frac{1}{8} Y(1 + y)$, we have finally

$$P_o^2 = \frac{16}{57} \quad \frac{g\, T_o^{11/2}}{1.75 \times 10^{21} Q}$$

or

$$P_o^2 = \frac{16}{57} \quad \frac{g}{7.61\, \theta_o^{11/2} Q}$$

It must be remarked that no point in the atmosphere corresponds to the pair of values (T_o, P_o). P_o is simply a convenient reference pressure, which turns out to be the value of P_e at $\tau = .23$.

We are now able to compute once and for all the run of t and p as functions of τ. These will be said to define the "Planck

model", and are exhibited in Table 2 and Fig. 2.

Emitted spectrum of Planck model

With the structure of the atmosphere known, the optical depth at any frequency can be found as a function of τ, provided the total monochromatic absorption coefficient is available in terms of T and P_e. From this the monochromatic emergent flux can be evaluated using the formal solution of the transfer equation. The present problem is to compute the profiles of the Balmer lines. At once a number of questions arise:

(1) What is the mechanism of line formation--absorption or scattering?

(2) What is the shape of the line absorption coefficient--i.e., what type of broadening predominates?

(3) What is the value of the line absorption coefficient?

Numerous investigations have made it clear that in the atmospheres of main-sequence B stars the dominant broadening mechanism is the Stark effect, and that in the line wings it is probably valid to treat it as a statistical phenomenon--i.e., to neglect the effects of motion of the perturbing ion relative to the H atom. It is less clear whether electrons must be considered as perturbers. The question of absorption vs. scattering has not been answered satisfactorily and it is not the purpose of this investigation to answer it. Pure absorption will be assumed and the observed central depth of the line will not be

used; in the wings the line depth is quite insensitive to this assumption. The contribution of electrons to the Stark broadening will be neglected.

The following notation will be used:

k = Planck mean opacity

k_λ = monochromatic continuous absorption coefficient

l_ν = monochromatic line absorption coefficient

$\eta_\nu = l_\nu / k_\lambda$; $n_\lambda = k_\lambda / k$

$d\tau$ = element of mean optical depth

$d\tau_\lambda = n_\lambda \, d\tau$

$d\tau_\nu = n_\lambda \, (1 + \eta_\nu) \, d\tau$

$B_\lambda(\tau)$ = monochromatic Planck function at integrated depth τ

$b_\lambda(\tau) = B_\lambda(\tau)/B_\lambda(0)$

H_ν = emergent monochromatic flux/4π in line

H_λ = emergent monochromatic flux/4π in continuum

$E_n(x) = \int_1^\infty \exp(-xy)\, y^{-n}\, dy$

In general a subscript ν denotes a quantity changing rapidly across an absorption line, while λ means the variation within the line can be neglected. To avoid confusion it must be emphasized here that quantities such as H_λ and B_λ are defined per unit <u>frequency</u> interval; i.e., $\int_0^\infty B_\lambda \, d\nu = B$, in contrast with the usual notation. In the continuum $H_\nu = H_\lambda$.

We start with the classical formal solution of the transfer equation:

$$H_\nu = \frac{1}{2} \int_0^\infty B_\lambda (\tau) E_2 (\tau_\nu) d\tau_\nu$$

or

$$\frac{2H_\nu}{B_\lambda (O)} = \int_0^\infty b_\lambda (\tau) E_2 (\tau_\nu) d\tau_\nu$$

Several approximations are customary. n_λ and η_ν are taken as constant with τ in the Milne-Eddington model, and $b_\lambda (\tau)$ is expanded as a linear function of τ. Then the integration becomes trivial and results in:

$$\frac{2H_\nu}{B_\lambda (O)} = \frac{1}{2} + \frac{\beta_\lambda}{3n_\lambda (1+\eta_\nu)} \quad \text{where} \quad \beta_\lambda = (db_\lambda / d\tau)_o .$$

Actual evaluation of n_λ, η_ν, and b_λ for a few relevant values of T and P_e shows, however, that the above approximations are rather poor. Therefore some much less drastic approximations were made:

$$n_\lambda (\tau) = n_\lambda (P_o, T_o) f(\tau) = y_\lambda f(\tau)$$

$$\eta_\nu (\tau) = \eta_\nu (P_o, T_o) g(\tau) = \chi_\nu g(\tau)$$

$$b_\lambda (\tau) = 1 + \beta (u_o) \rho (\tau) \qquad \rho (o) = 0$$

where $u_o = hc/\lambda kT_o$. These approximations were, in fact, suggested

by graphs of the functions in question. The temperature and pressure dependence is as follows:

$$k \sim P_e T^{-11/2} N(T)$$

$$k_\lambda \sim P_e T^{-5/2} D_2(T) (1 - e^{-u})$$

$$l_\nu \sim P_e^2 T^{-7/2} 10^{3.40\theta} (1 - e^{-u})$$

where only the leading term in the Stark-broadened line absorption coefficient has been retained.

$$D_2(T) = \sum_{n=3}^{\infty} \frac{1}{n^3} e^{u_n} + \frac{1}{2u_1}$$

and this has been tabulated, for example, by Unsöld (26).

Thus we have

$$n_\lambda \sim T^{-3} \frac{D_2(T)}{N(T)} (1 - e^{-u})$$

$$\eta_\nu \sim P_e \frac{10^{3.40\theta}}{T D_2(T)}$$

and these were plotted logarithmically against temperature. These plots were remarkably linear; in the range $T = 12,000^\circ$ to $25,000^\circ$ they were fitted by

$$n_\lambda \sim T^{2.36} , \qquad \eta_\nu \sim P_e T^{-2.95}$$

with maximum errors of 7% and 3% respectively. Hence we adopt

$$f(\tau) = t^{2.36},$$

$$g(\tau) = pt^{-2.95}.$$

To get τ_ν as a function of τ, we note that

$$\tau_\nu(\tau) = y_\lambda \int_0^\tau f(\tau')\,d\tau' + x_\nu y_\lambda \int_0^\tau g(\tau')f(\tau')\,d\tau'$$

so the computation of two more functions is necessary:

$$F(\tau) = \int_0^\tau f(\tau')\,d\tau'$$

$$G(\tau) = \int_0^\tau g(\tau')f(\tau')\,d\tau'$$

and in terms of these

$$\tau_\nu / y_\lambda = F + x_\nu G.$$

Finally $b_\lambda = (e^{u_o} - 1)/(e^{u_o/t} - 1)$ was computed for $u_o = 2,\ 2.5,\ 3.0$ and found to be represented to within 3% by an expression of the form

$$b_\lambda = 1 + \beta(u_o)\,\rho(\tau)$$

where $1 + \rho(\tau) = b_\lambda\ (u_o = 2.5)$,

and $\log \beta(u_o) = .088\,(u_o - 2.50)$.

The functions $F(\tau)$, $G(\tau)$, and $\rho(\tau)$ are given in Table 2 and Fig. 2 . By way of comparison, it may be remarked that in the Milne-Eddington model all three are proportional to τ .

The flux integral may now be written as

$$\frac{2H_\nu}{B_\lambda(0)} = \int_0^\infty b_\lambda(\tau) E_2(\tau_\nu)\, d\tau_\nu$$

$$= \frac{1}{2} + \beta(u_o) \int_0^\infty \rho(\tau) E_2(\tau_\nu)\, d\tau_\nu$$

$$= \frac{1}{2} + \beta(u_o)\, \varphi(x_\nu, y_\lambda).$$

Before evaluating the quantity φ some attention must be given to the ranges of values assumed by x_ν and y_λ . Clearly x_ν will vary from ∞ in the center of a strong line to 0 in the continuum. y_λ , the value of n_λ at the boundary temperature, is given by

$$y_\lambda = .75 \left(\frac{\Theta_o}{.300}\right)^{-2.36} \left(\frac{\lambda}{4300}\right)^3$$

and hence ranges from about .40 to about 1.40 for the early Balmer lines (excluding Hα) and boundary temperatures of 12,500° to 18,500°.

The integral φ was evaluated for

$y_\lambda = 0.6,\ 1.0,\ 1.4$

$x_\nu = 0,\ .10,\ .30,\ 1.0,\ 3.0,\ 10,\ 30,\ \infty$

using a four-point Gaussian integration formula with representative points and weights computed by Reiz (30).

At any point in the line profile the depth in units of the continuum is

$$A_\nu = \frac{H_\lambda - H_\nu}{H_\lambda} = \frac{\beta(u_o)\left[\varphi(0, y_\lambda) - \varphi(x_\nu, y_\lambda)\right]}{\frac{1}{2} + \beta(u_o)\,\varphi(0, y_\lambda)}$$

and it is convenient to express this in terms of the "central depth of a strong line":

$$A_o = A_\nu(x_\nu = \infty) = \frac{\beta(u_o)\,\varphi(0, y_\lambda)}{\frac{1}{2} + \beta(u_o)\,\varphi(0, y_\lambda)} = A_o(\Theta_o, \lambda).$$

The quotation marks are intended to emphasize the fact that A_o is not to be taken literally; near the line center the depth is sensitive to departures from thermodynamic equilibrium, changes in $T(\tau)$ due to the blanketing effect, and breakdown of the statistical Stark broadening of the line absorption coefficient--none of which have been taken into account. In general it is expected that A_o will be smaller than the observed central depth.

From the above expressions we get

$$A_\nu / A_o = 1 - \varphi(x_\nu, y_\lambda) / \varphi(0, y_\lambda).$$

This quantity was found to be independent of y_λ to within the accuracy

of the computations and is denoted by $a(x_\nu)$. Thus

$$A_\nu = A_o(\theta_o, \lambda)\, a(x_\nu)$$

where A_o and a are given by Fig. 3.

The line profile is now obtained by specifying the dependence of x_ν on wavelength within the line. For the leading term in the Stark wings, this dependence is $x_\nu \sim (\Delta\lambda)^{-5/2}$ where $\Delta\lambda$ = distance from line center in Å. It is therefore convenient to write

$$x_\nu = x_1 (\Delta\lambda)^{-5/2} ; \quad \Delta\lambda = (x_1/x_\nu)^{2/5}$$

and plot A_ν against $\Delta\lambda$ with x_1 and A_o as parameters. The profiles thus obtained are all, in a sense, identical; they differ only in scale. A_o fixes the scale in depth and x_1 fixes the scale in wavelength.

Finally, x_1 must be related to the Stark constant of the line and the parameters of the atmosphere. The atomic absorption coefficient in the wings, considering statistical Stark broadening by ions only, is given by

$$\alpha_\nu = C_n P_e \theta (\Delta\lambda)^{-5/2} \text{ cm}^2 \text{ per atom in } (n = 2)$$

where $\Delta\lambda$ is in Å and the constant C_n is found, for example, from the work of Verweij (31):

Line	$C_n \times 10^{18}$
H γ	2.79
H δ	1.95

Referring the absorption coefficient to a gram of stellar material, considering the abundance of hydrogen, and dividing by the continuous absorption coefficient due to hydrogen and helium, we get

$$\eta_\nu = K_n \frac{X}{R} \frac{P_e}{100} \left(\frac{\Theta}{.300}\right)^{2.95} (\Delta\lambda)^{-5/2}$$

where

$$\log K_n = 18.83 + \log C_n + 3 \log \frac{4300}{\lambda}$$

$$= \begin{cases} 1.27 \ (H\gamma) \\ 1.19 \ (H\delta) \end{cases},$$

$$R = X + \frac{1}{4} Yy.$$

Hence

$$x_1 = K_n \frac{X}{R} \frac{P_o}{100} \left(\frac{\Theta_o}{.300}\right)^{2.95}$$

and at a given temperature the overall width of the line is proportional to $x_1^{2/5}$, so

$$\Delta\lambda \sim P_o^{2/5} \sim g^{1/5}$$

as was obtained by Verweij.

TABLE II

PLANCK MODEL ATMOSPHERE

τ	t^4	p	F	G	ρ
0	1.000	0	0	0	0
.01	1.015	.187	.010	.002	.01
.02	1.030	.263	.021	.004	.02
.03	1.045	.328	.031	.006	.03
.04	1.060	.388	.042	.010	.04
.05	1.075	.435	.052	.014	.05
.10	1.15	.620	.105	.039	.10
.20	1.30	.933	.217	.117	.19
.30	1.45	1.19	.340	.220	.28
.40	1.60	1.43	.465	.325	.36
.60	1.90	1.90	.748	.63	.51
.80	2.20	2.35	1.05	1.01	.65
1.00	2.50	2.79	1.38	1.44	.78
1.20	2.80	3.24	1.74	1.98	.89
1.40	3.10	3.72	2.12	2.61	1.00
1.60	3.40	4.18	2.53	3.27	1.11
1.80	3.70	4.63	2.94	3.99	1.21
2.00	4.00	5.09	3.38	4.77	1.30
2.50	4.75	6.28	4.56	7.06	1.52
3.00	5.50	7.50	5.88	9.78	1.72

FIGURE 2
PLANCK MODEL ATMOSPHERE

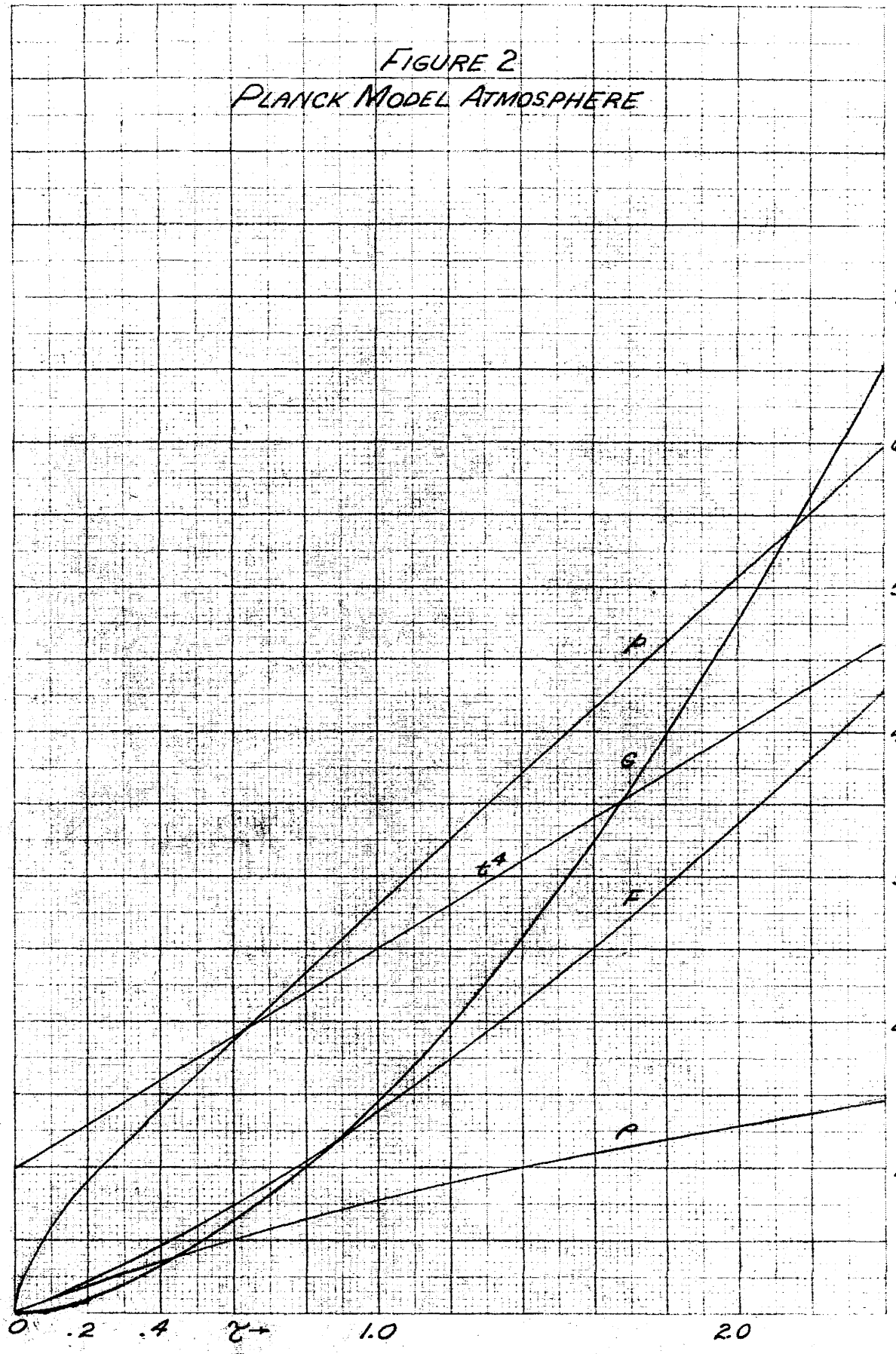

FIGURE 3

DEPTH / CENTRAL DEPTH $a(x_v)$

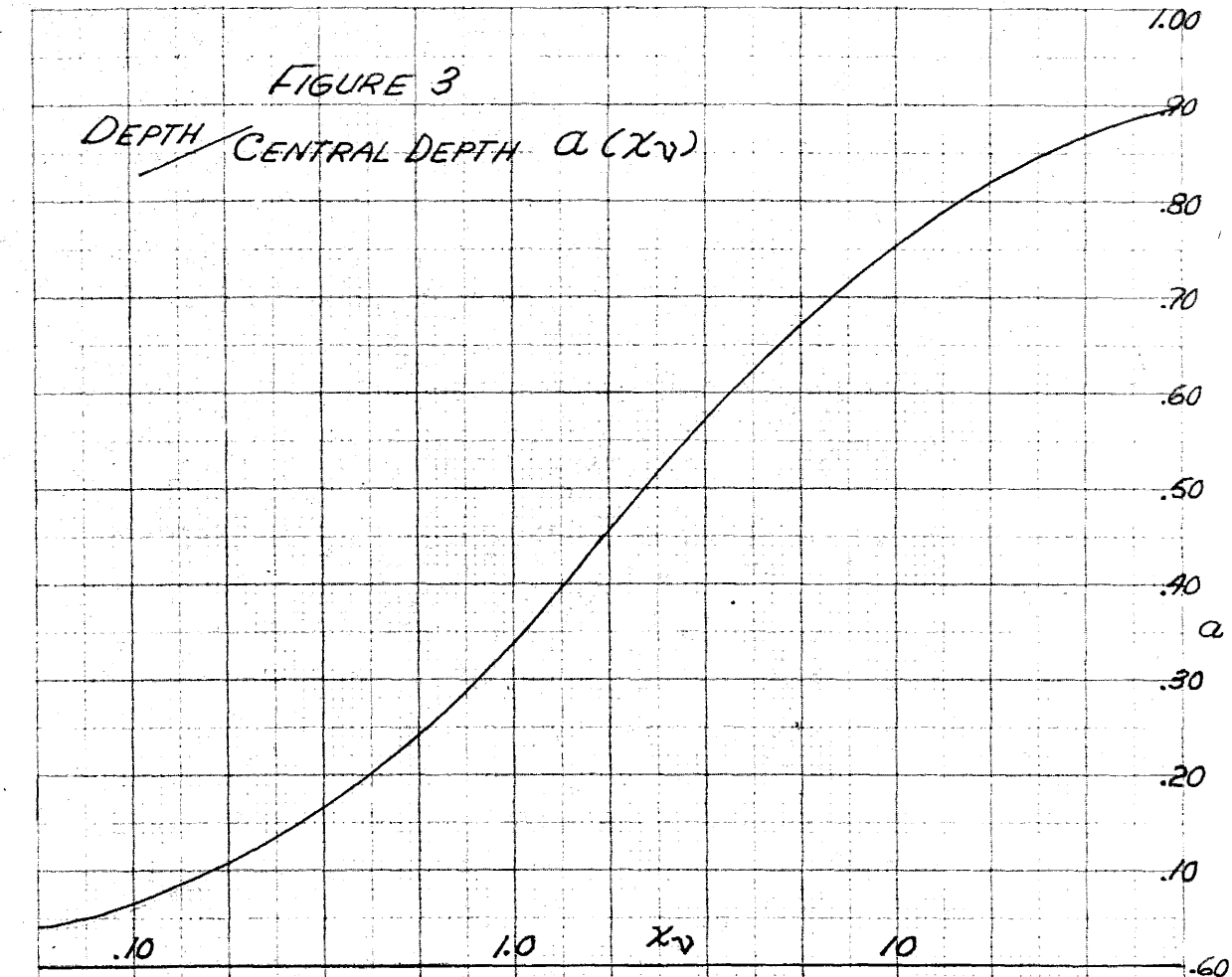

CENTRAL DEPTH $A_0(\theta_0, \lambda)$

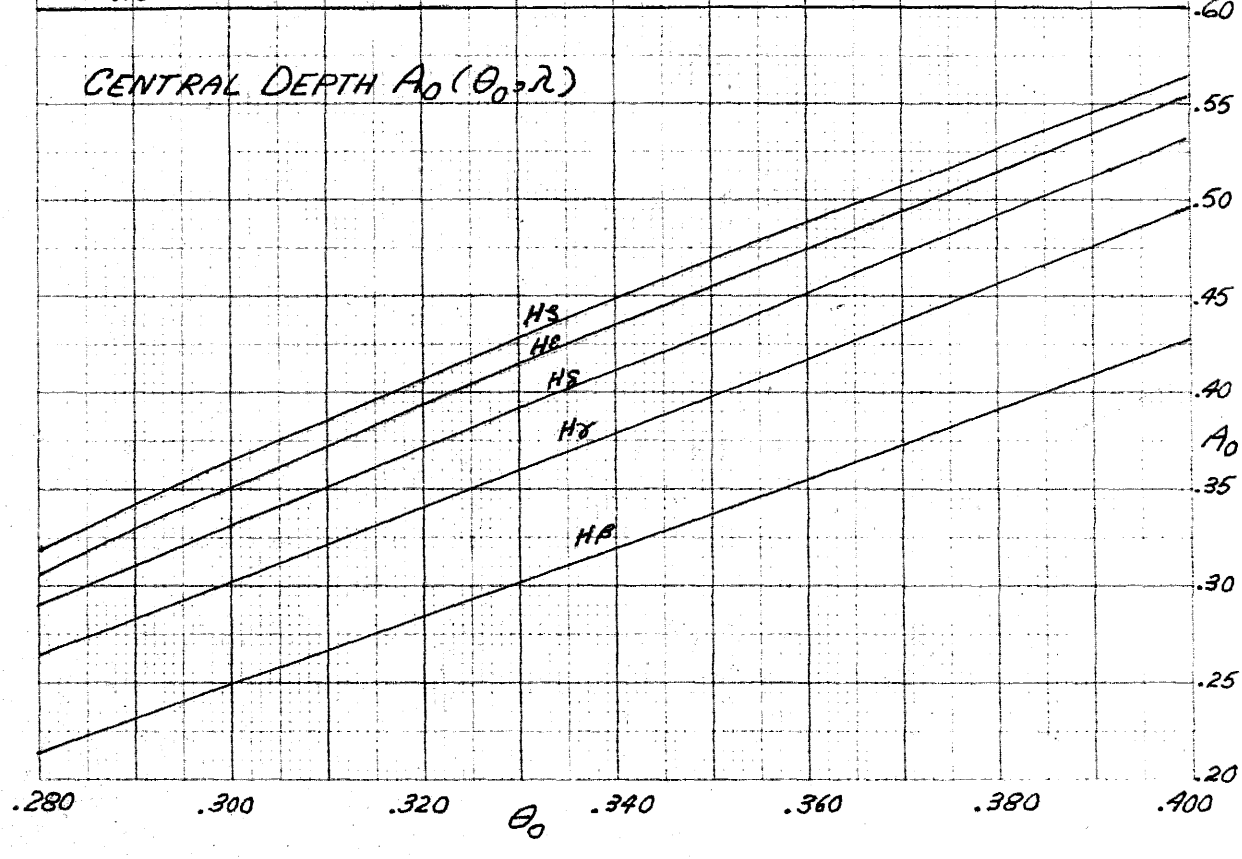

Fitting observed Balmer profiles

For purposes of direct visual comparison of computed and observed profiles, a family of curves $A_\nu(\Delta\lambda)$ with x_1 as parameter was plotted for each of several values of A_o, using translucent paper. Ideally, of course, any observed profile should fit a particular one of these curves and thus allow the determination of both x_1 and A_o. However, for reasons mentioned earlier, the line cores are not expected to be correctly predicted. In practice the part of the profile for which $A_\nu = .05$ to $.20$ was used; the extreme wings are too uncertain observationally to be useful. The agreement in the region of fitting was quite good for more than one value of A_o. Hence for a given observed profile several values of x_1, corresponding to different A_o, were read off. For a given line A_o depends only on Θ_o, and it was found that

$$\frac{2}{5} \log x_1 = D_1 - D_2\Theta_o$$

to within the uncertainty of fitting, where D_1 depends on the observed profile and $D_2 = 1.60$ for all profiles.

In this way the values of D_1 for Hγ and Hδ were found for each star. The data for Hδ were reduced to Hγ and the mean of the two was used. In what follows, D_1 will refer to this mean. The uncertainty in the determination of D_1 is estimated as $.03$. Since

$$\log x_1 (H\gamma) = 0.81 + \log P_o + 2.95 \log \Theta_o + \log \frac{X}{R}$$

from the preceding section, we get

$$\frac{5}{2} D_1 + \log \frac{R}{X} = 0.81 + \log P_o + 2.95 \log \Theta_o + 4.00 \Theta_o .$$

Predicted He and Si equivalent widths

We proceed by the method of weighting functions as developed by Unsöld (32) for weak lines formed in local thermodynamic equilibrium. The line depth is then

$$A_\nu = \int_0^\infty G_1(\tau_\lambda)\ \eta_\nu(\tau_\lambda)\, d\tau_\lambda$$

and the equivalent width in wavelength units is

$$W = \int_{line} A_\nu\, d\lambda = \frac{\pi e^2}{mc^2}\ \lambda^2 f \int_0^\infty N_{rs}(\tau)\, G_1(\tau_\lambda)\, \frac{d\tau_\lambda}{k_\lambda}$$

where

N_{rs} = no. atoms per gm of stellar material in initial state of line

$$G_1(\tau_\lambda) \equiv \frac{\phi(\tau_\lambda) - B_\lambda(\tau_\lambda)\, E_2(\tau_\lambda)}{\int_0^\infty B_\lambda(\tau_\lambda)\, E_2(\tau_\lambda)\, d\tau_\lambda}$$

$$\phi(\tau_\lambda) \equiv \int_{\tau_\lambda}^\infty B_\lambda(\tau_\lambda')\, E_1(\tau_\lambda')\, d\tau_\lambda' \ .$$

If G_1 is expressed in terms of τ for the Planck model atmosphere, we get

$$\left[\frac{1}{2\beta(u_o)} + \varphi(o, y_\lambda)\right] G_1(\tau) = \int_\tau^\infty E_2(\tau_t)\, \frac{d\rho(\tau)}{d\tau}\, d\tau \equiv \Gamma(\tau)$$

This was evaluated by numerical integration for $y_\lambda = 0.6,\ 1.0,\ 1.4$ and found to be very closely exponential in τ. Thus

$$\Gamma(\tau) = \Gamma(0)\, 10^{-\gamma\tau}$$

with $\gamma = .42 + .80\, y_\lambda$ and $\frac{1}{\Gamma(0)} = .94 + 2.25\, y_\lambda$.

Expressing f in terms of S, using the Boltzmann equation, and inserting all constants, we have for an unsaturated line

$$W/\lambda = 1.62 \times 10^{6} \frac{X_z}{A_z} \frac{S}{b_r} G_1(0) \frac{N_r}{N_z} 10^{-\Theta\chi_s} 10^{-\gamma\tau} \frac{d\tau}{k}$$

where X_z = abundance by mass of element Z

A_z = atomic mass in amu

b_r = partition function

$\frac{N_r}{N_z}$ = Saha factor = fraction of atoms in right ionization stage.

Using the above expression, the ratio $\left(\frac{W/\lambda}{S}\right)_{\text{Si III}} \Big/ \left(\frac{W/\lambda}{S}\right)_{\text{Si II}}$ for the λ4560 multiplet of Si III and the λ4130 multiplet of Si II, which will be called D_4, was computed as a function of Θ_o and P_o. The result is

$$\log D_4 = 10.49 - 23.1\, \Theta_o - \log P_o$$

within .05 in the log, for $\Theta_o = .250$ to .400.

With the aid of Wrubel's theoretical Milne-Eddington curves of growth (33), it may be seen that the observed Si lines are

not weak enough to be considered unsaturated; however, they are not so strong that the value of the damping constant is important, and the assumption that saturation effects are equal for a Si II line and a Si III line of equal W/λ appears admissible. Then the observed W/λ 's can be reduced to unsaturated W/λ 's, using the curve of growth, to get D_4. This procedure, as mentioned before, is essentially a replacement of η_o by its weighted mean value in using the curve of growth, and is expected to be more accurate than either the usual curve of growth (which neglects stratification) or the weak-line weighting-function method (which neglects saturation), while less accurate than the saturated weighting functions introduced by Pecker (16). From the internal agreement among the Si lines, the observational uncertainty in $\log D_4$ is estimated as .10.

The quantity $\frac{W/\lambda}{S}$ for He I λ 3927, which will be called D_3, was also computed. For the hotter part of the range of interest, where He II $\gg$ He I, D_3 is independent of P_o and its temperature dependence is slow; at the cool end D_3 is relatively sensitive to both P_o and θ_o. For a line such as λ 3927 with a half-width of over 2 Å and an observed central depth on the order of 10%, it is clear that saturation can play no important part. As a check, plots similar to those used by Unsöld (34) were made showing the observed $\frac{W/\lambda}{S}$ (properly corrected for the wavelength dependence of k_λ) for the members of the various helium series; these indicated a more or less

unique limiting value for the higher members, which was used rather than the value for λ 3927 alone. The observational uncertainty in log D_3 is about .05.

An interesting byproduct of the above computations is the representative optical depth τ_λ^* at which the lines are predominantly formed (8). For the He I lines in the hotter stars, and for the Si II lines, $\tau_\lambda^* \approx .4$; for the Si III lines $\tau_\lambda^* \approx .8$.

FIGURE 4

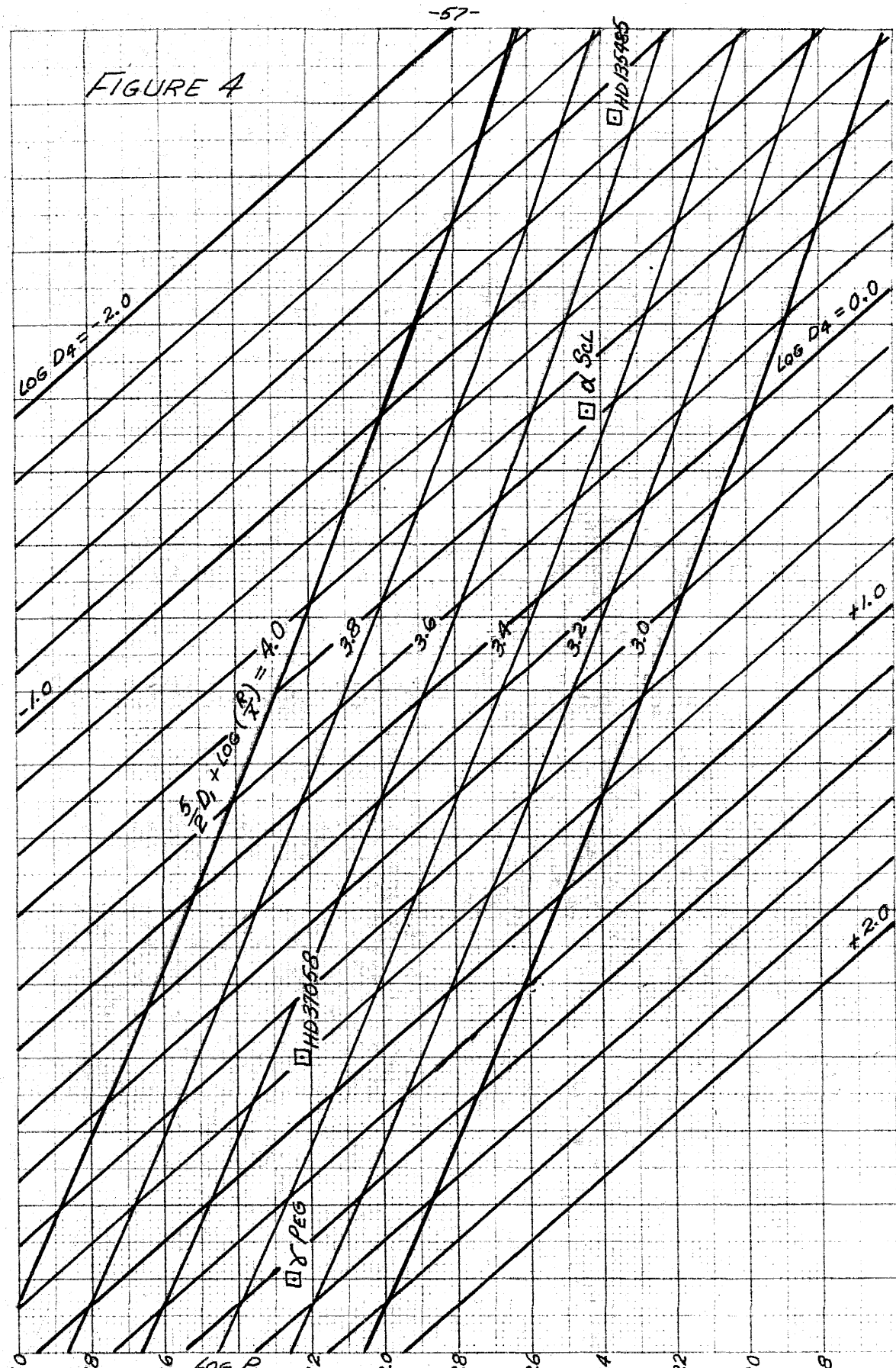
LOG D4 = -2.0
-1.0
5/2 D1 + LOG (R/r) = 4.0
3.8
3.6
3.4
3.2
3.0
LOG D4 = 0.0
+1.0
+2.0
HD 135485
α Sct
HD 37058
γ Peg
4.0
3.8
3.6
LOG D0
3.2
3.0
2.8
2.6
2.4
2.2
2.0
1.8
.420
.400
.380
.360
.340
.320
.300
.280
.260
.240
θo

FIGURE 5

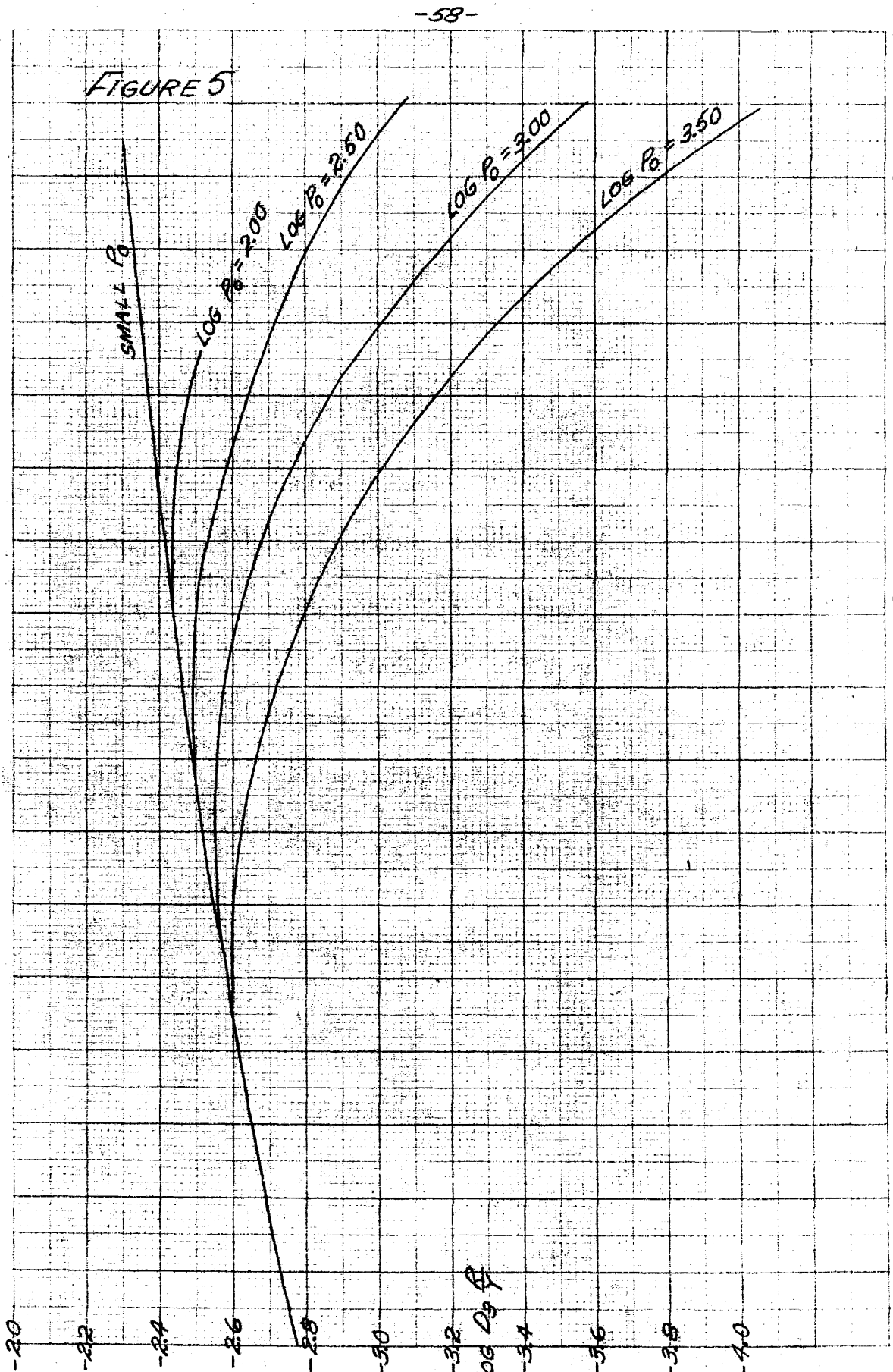
SMALL P_0
LOG P_0 = 2.00
LOG P_0 = 2.50
LOG P_0 = 3.00
LOG P_0 = 3.50
LOG D_g $\frac{P}{P_0}$
θ_0
-2.0
-2.2
-2.4
-2.6
-2.8
-3.0
-3.2
-3.4
-3.6
-3.8
-4.0
.240
.260
.280
.300
.320
.340
.360
.380
.400
.420

CHAPTER V

Determination of atmospheric parameters

We now have at our disposal all the relations necessary to find, from the observed data D_1, D_3, D_4, the parameters Θ_o, P_o, Y of the atmosphere. It is convenient to do this graphically and no loss of accuracy is suffered thereby. Fig. 4 shows lines of constant $\frac{5}{2} D_1 + \log \frac{R}{X}$ and lines of constant D_4 in the (Θ_o, log P_o)plane; Fig. 5 shows lines of constant P_o in the $\left(\Theta_o, \log \frac{RD_3}{Y}\right)$ plane. An initial guess of $\log \frac{R}{X}$ (e. g., zero) gives initial values of Θ_o and log P_o which are used to find $\log \frac{R}{Y}$. Then, recalling that

$$R = X + \frac{1}{4} Yy = 1 - Y(1 - \frac{1}{4} y)$$

the value of Y is found. Since, strictly speaking, the proper mean value of y is not defined when it changes through the atmosphere, there is a small uncertainty in the derived Y; but this uncertainty is smaller than the observational uncertainty in D_3 except when Y is quite large (> .50). A new value of $\log \frac{R}{X}$ is now available and improved values of Θ_o and P_o result; one such iteration generally proves to be quite sufficient.

Finally the value of g may be obtained from the relation which was derived earlier:

$$P_o^2 = \frac{16}{57} \quad \frac{g}{7.61\, \Theta_o^{11/2}\, Q}$$

or

$$\log g = 1.43 + 2 \log P_o + \frac{11}{2} \log \Theta_o + \log Q$$

with $Q = X + \frac{1}{8} Y (1 + y)$.

Values of the data and resulting parameters are given below.

Star	γ P_{eg}	HD 37058 HD 37129	α S_{cl}	HD 135485
D_1	1.31	1.41	1.38	1.45
$\log D_3$	-3.6	-3.5	-4.1	-3.2
$\log D_4$	1.47	0.79	-0.45	-1.31
Θ_o	.250	.280	.368	.408
$\log P_o$	3.25	3.23	2.44	2.36
Y	.13	.13	.03	.34
log g	4.57	4.80	3.92	3.86

Abundances of other elements

The absolute abundance by mass, X_z, of an element can be related to the observed equivalent widths of its lines through the curve of growth. In the Milne-Eddington approximation $\log \frac{W}{\lambda} \frac{c}{v}$ is plotted against $\log \eta_o$, which is the value of η at the line center

for zero damping, taken as constant through the atmosphere. Using the Boltzmann equation and inserting all physical constants,

$$\eta_o = 10^{5.96} \; \frac{1}{k_\lambda} \; \frac{N_r/b_r}{N_z} \; \frac{X_z}{A_z} \; \frac{c}{v} \; S \; 10^{-\Theta_{ex}\chi_s}$$

where k_λ, Θ_{ex}, etc., have values appropriate to some mean depth in the atmosphere. In practice it is convenient to plot log W/λ against $S' \cdot 10^{-\Theta_{ex}\chi_s}$ (where $S' = S \; \frac{k_{4300}}{k_\lambda}$) for all lines of an ion, and then to fit the theoretical curve by horizontal and vertical shifts whose sizes determine X_z and $\frac{c}{v}$ respectively, while the effective damping constant a is found by choosing the one of a family of theoretical curves which fits best. The excitation temperature Θ_{ex} is chosen so as to minimize the scatter in the observed curve.

In the present study it soon became clear that the number of available lines was too small to define complete curves of growth and that the spread in χ_s among lines of any one ion was insufficient for the determination of Θ_{ex}. Therefore only one parameter, the abundance X_z, was determined from the curve of growth for each ion; all other quantities were evaluated at a depth of $\tau_{4300} \approx .35$ in the appropriate model atmosphere. This choice of depth is based on the behavior of the Si II lines in the weighting-function treatment. For all ions log a was taken as -1.8.

Blended multiplets such as λ 3876 of C II were treated twice: as if completely blended ($S_{blend} = \sum S_{components}$) and as if

completely unblended ($W_{blend} = \sum W_{components}$). Both points were plotted on the curve of growth and the extent of blending could then be roughly seen. Blends between elements could generally be assigned to a single contributor after the unblended lines were plotted.

Absolute abundances of C, N, O, Si, and S were obtained, using the theoretical line strengths computed earlier, for HD 37058 and HD 135485. In addition the abundance of Mg was found for HD 135485. The results follow:

Element	$\log X_z$	
	HD 37058	HD 135485
C	-3.6	-2.8
N	-4.0	-2.4
O	-3.3	-1.4
Mg	----	-4.0
Si (II)	-4.2	-3.1
Si (III)	-4.2	-3.1
S	-3.7	-3.8

FIGURE 6α
CURVES OF GROWTH
HD37058

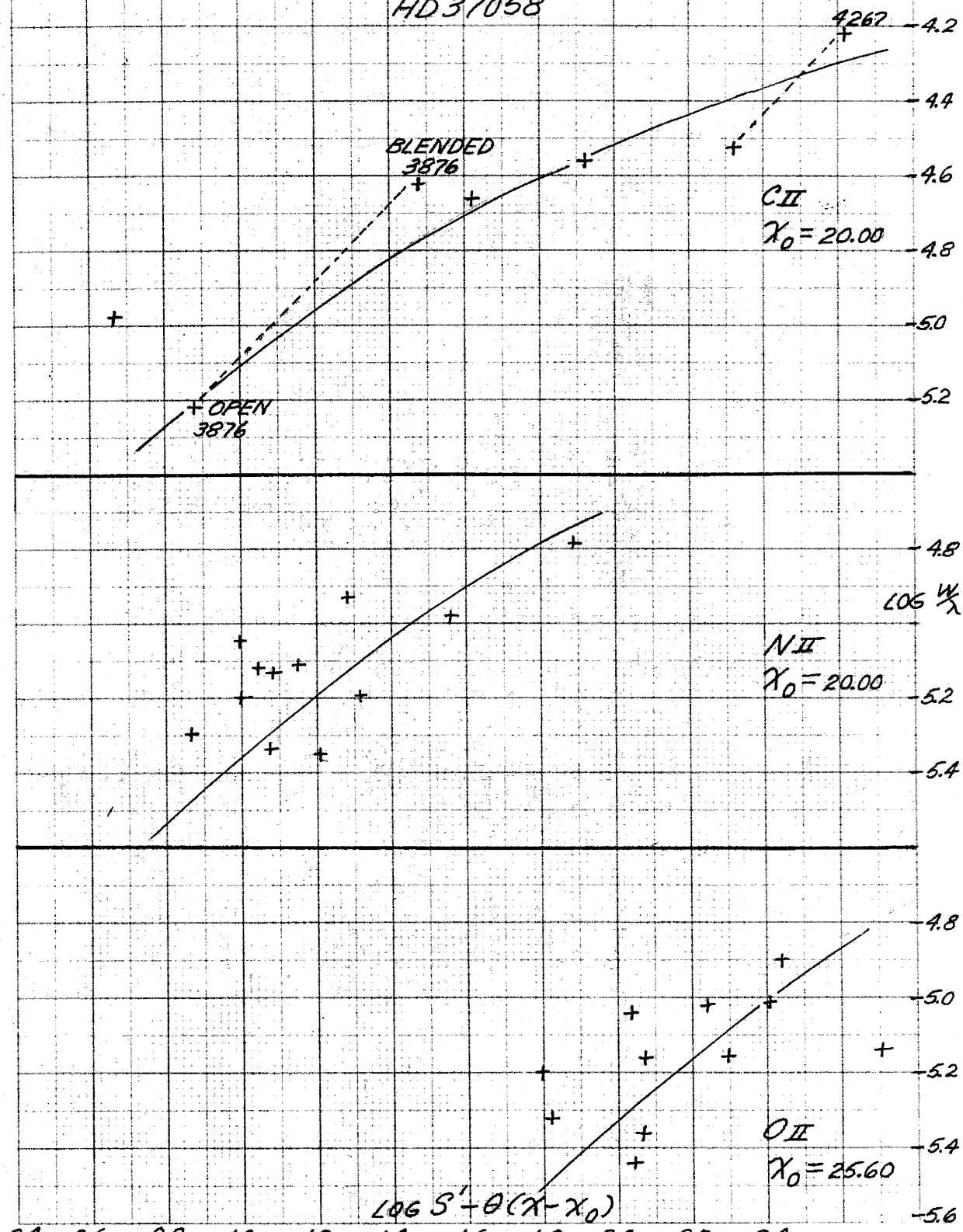

FIGURE 66
CURVES OF GROWTH
HD 37058

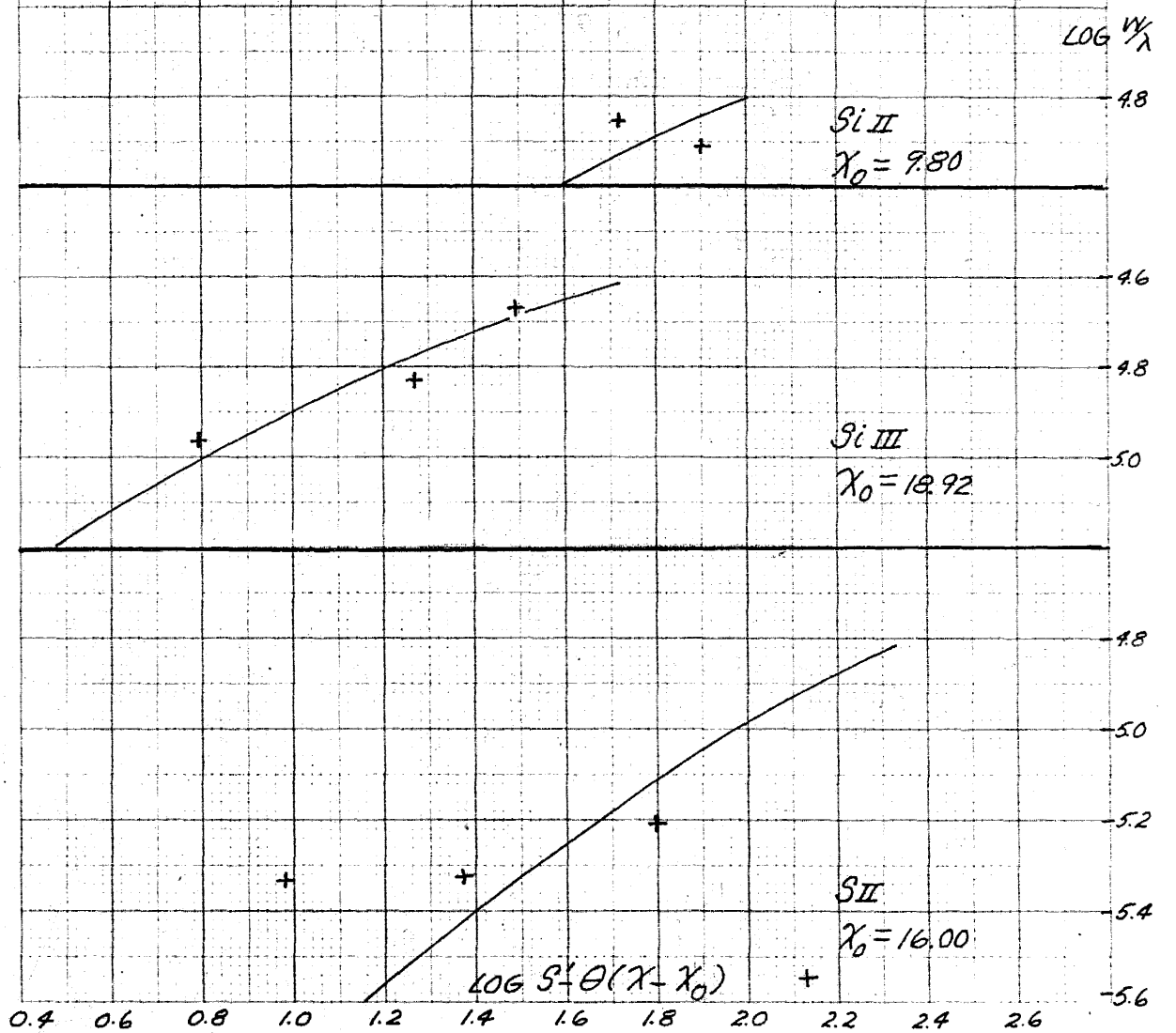

FIGURE 6c
CURVES OF GROWTH
HD135485

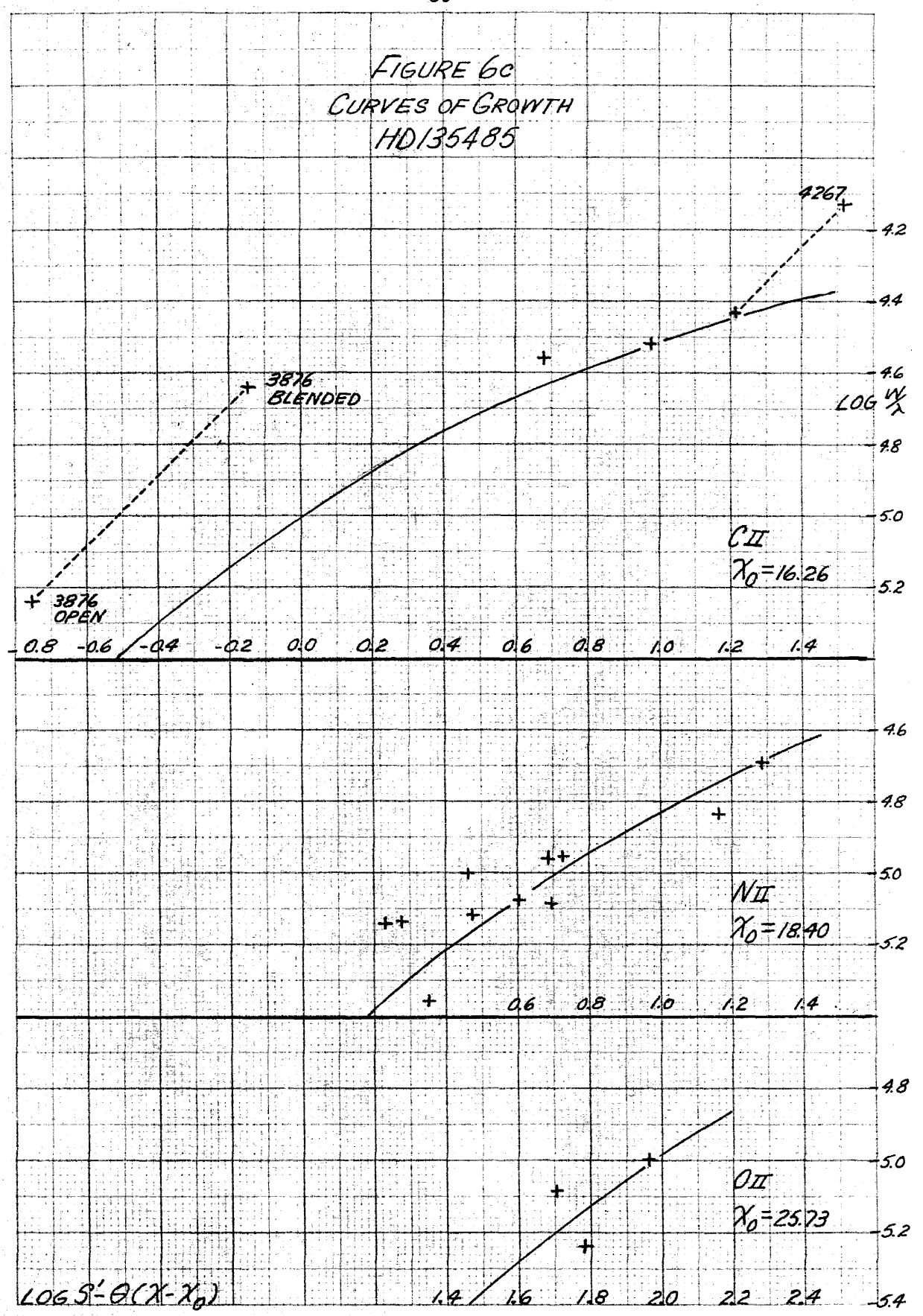

FIGURE 6d
CURVES OF GROWTH
HD135485

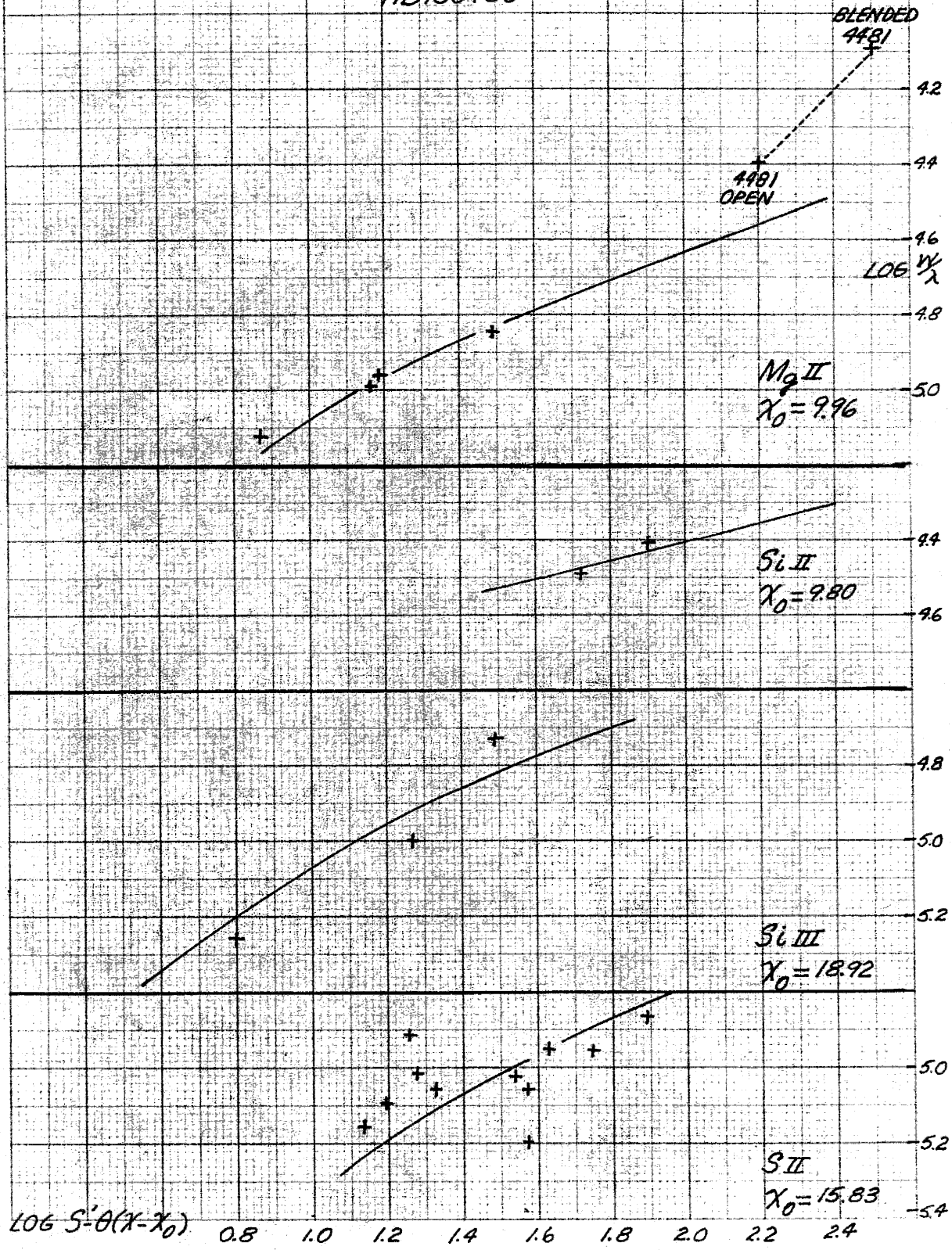

Discussion of results

We first examine the observational uncertainties of the atmospheric parameters, which may be estimated using the graphs and the probable errors of the data. Treating the latter as independent errors, the probable errors in the results are roughly

$$\Delta\Theta_o = \pm .010 \qquad \Delta \log P_o = \pm .10$$

$$\Delta \log g = \pm .20$$

$$\Delta \log Y = \pm .10 \left(\begin{matrix}\gamma \text{ Peg} \\ \text{HD } 37058\end{matrix}\right), \pm .15 \left(\begin{matrix}\alpha \text{ Scl} \\ \text{HD } 135485\end{matrix}\right).$$

The probable error in the abundance determinations of other elements is estimated from the scatter in the curves of growth as

$$\Delta \log X_z = \pm .20$$

where the influence of the uncertainties in Θ_o and $\log P_o$ has been taken into account.

A comparison of the results for γ Peg with those obtained by Neven (8) shows that although our helium abundances agree closely, our models do not; his model is characterized by considerably lower values of the temperature, electron pressure, and surface gravity. Neven's Θ_o, which refers to the boundary of his unmodified grey model, should be directly comparable to my Θ_o. His value of P_e at $\tau = .23$, which corresponds to my P_o, may be chosen as a "typical" electron pressure. Neven's results follow:

$\Theta_o = .365$ $\quad$ $Y = .14$

$\log P_o = 2.53$ $\quad$ $\log g = 3.63$

These values differ considerably from mine, with the exception of Y.

A large part of the discrepancy in log g is due simply to Neven's use of a smaller mean absorption coefficient. Using his values of Θ_o, P_o, and Y and the Planck mean, we find log g = 4.04. A slightly different comparison shows that at the same temperature and pressure the Rosseland mean opacity for the mixture ($Y \approx .41$) used by Neven in the construction of his models is smaller, by a factor of about three, than the Planck mean opacity for the final composition.

Neven also concluded that the inclusion of electrons as a broadening agent in the Balmer lines was consistent with his observations, while I have included only protons; hence I require a larger electron pressure than does Neven to describe the same Balmer profile.

Finally, the two models were derived using rather different observational data. The material available to Neven did not include the Si lines used in the present study; accordingly, I have evaluated the Si III/Si II line ratio for Neven's model, using the weighting function computed by him. The result is that $\log D_4 \approx -0.40$; this agrees well with the value -0.47 obtained from my own weighting

function with his Θ_o and P_o, but disagrees violently with my observed log D_4 = 1.47. It is felt that the Balmer discontinuity, which Neven used essentially as a temperature indicator, is not as sensitive as the Si III/Si II line ratio.

In view of the large differences between the two models, the close agreement of the derived helium abundances must be regarded as fortuitous; Fig. 5 indicates that the models are located on opposite sides of the maximum of helium line strength with respect to temperature.

The question of the absolute magnitudes of the peculiar stars may now be answered on the basis of simple assumptions concerning their interiors. In the first place, we assume the Cowling model, equal content of heavy elements, and thorough mixing for both peculiar and standard stars. Using the derived atmospheric parameters, a straightforward application of the mass-radius-luminosity law yields the following relations among bolometric magnitudes:

$$M(\text{HD } 37058) = M(\gamma \text{ Peg}) + 1.4$$

$$M(\text{HD } 135485) = M(\alpha \text{ Scl}) + 0.8$$

On the other hand, if the interior of HD 135485 were devoid of hydrogen,

$$M(\text{HD } 135485) = M(\alpha \text{ Scl}) + 2.4$$

These (oversimplified) considerations place both peculiar stars

below the main sequence at about spectral type B3 and B6 respectively.

The abundances obtained from the curves of growth are exhibited in Fig. 7. For comparison the results of Neven and Aller for γ Peg are also shown. The outstanding anomaly is the comparatively low abundance of O relative to C and N in HD 37058, the titanium-rich star, in accord with the weakness of the O II lines in this star noticed in the qualitative survey.

FIGURE 7

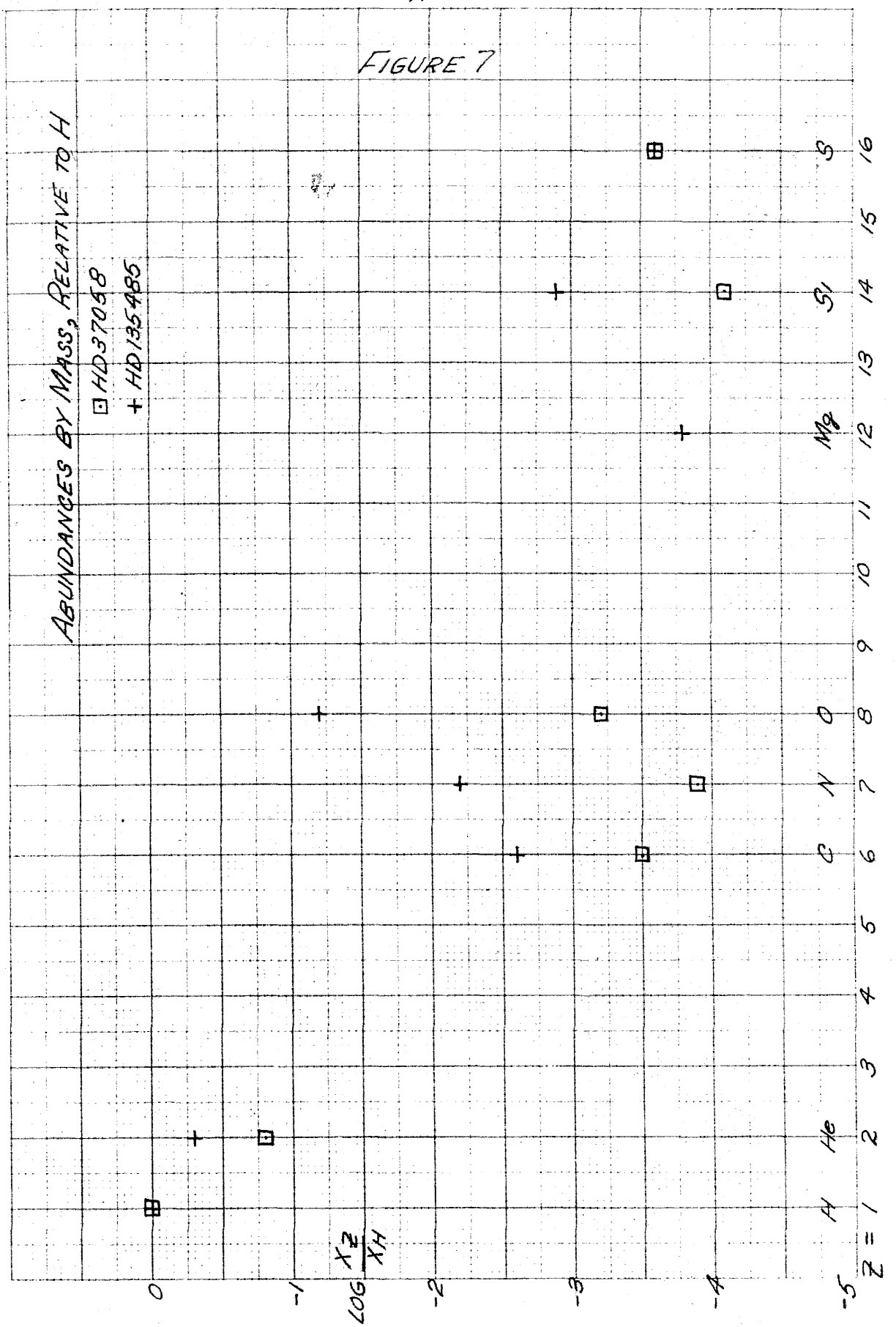
ABUNDANCES BY MASS, RELATIVE TO H
⊡ HD37094
+ HD135485
LOG X_Z / X_H
0
-1
-2
-3
-4
-5
Z = 1
2
3
4
5
6
7
8
9
10
11
12
13
14
15
16
H
He
C
N
O
Mg
Si
S

REFERENCES

1. e. g. O. Struve, Stellar Evolution, Princeton Univ. Press (1950)
2. A. B. Underhill, Contr. Dom. Ap. Obs. #30 (1953)
3. R. E. Wilson, General Catalogue of Stellar Radial Velocities, Carnegie Inst. of Wash., Pub. #601 (1953)
4. S. Sharpless, Ap. J. 116, 251 (1952)
5. F. J. Neubauer, Ap. J. 97, 300 (1943)
6. J. A. Pearce and R. M. Petrie, Pub. Dom. Ap. Obs. VIII, #15 (1951)
7. L. H. Aller, Ap. J. 109, 244 (1949); Astrophysics, vol. I, New York: Ronald Press (1953)
8. L. Neven, Thesis, Liège (1952); L. Neven and C. de Jäger, B.A.N. XII, 103 (1954)
9. C. E. Moore, A Multiplet Table of Astrophysical Interest (Revised), Contr. Princeton Univ. Obs. #20 (1945)
10. O. Struve, Ap. J. 74, 225 (1931); 90, 699 (1939)
11. H. N. Russell and R. J. Lang, Ap. J. 66, 25 (1927)
12. W. W. Morgan, P. C. Keenan, and E. Kellman, An Atlas of Stellar Spectra, Univ. of Chicago Press (1943)
13. P. C. Keenan and W. W. Morgan, in Astrophysics (J. A. Hynek, ed.), McGraw-Hill Book Co. (1951)
14. A. B. Underhill, Ap. J. 107, 337 (1948)
15. R. Michard, Ann. d'Ap. 12, 291 (1949)
16. J.-C. Pecker, Contr. Inst. Ap. Paris B, #65 (1951)
17. J. K. McDonald, Pub. Dom. Ap. Obs. IX, #9 (1953)
18. A. B. Underhill, Pub. Med. Køb. Obs. #151 (1950)

19. D. R. Bates and A. Damgaard, Phil. Trans. Roy. Soc. A, 242, 101 (1949)

20. R. H. Garstang, M.N. 114, 118 (1954)

21. E. U. Condon and G. Shortley, The Theory of Atomic Spectra, London: Cambridge Univ. Press (1935), ch. IX

22. L. Goldberg, Ap. J. 82, 1 (1935); 84, 11 (1936)

23. H. E. White and A. Y. Eliason, Phys. Rev. 44, 753 (1933)

24. K. O. Wright, Pub. Dom. Ap. Obs. XIII, #1 (1951)

25. C. Mark, Phys. Rev. 72, 558 (1947)

26. A. Unsöld, Physik der Sternatmosphären, Berlin: Julius Springer (1938), pp. 118-121

27. M. Rudkjøbing, Pub. Med. Køb. Obs. #145 (1947)

28. S.-S. Huang, Ap. J. 108, 354 (1948)

29. L. Goldberg, Ap. J. 90, 414 (1939)

30. A. Reiz, Arkiv för Astron., Bd. 1, Häfte 2, 147 (1950)

31. S. Verweij, Pub. Astron. Inst. Univ. Amst. #5 (1936)

32. A. Unsöld, Sternatmosphären, p. 253

33. M. Wrubel, Ap. J. 109, 66 (1949)

34. A. Unsöld, Zs. f. Ap. 21, 22 (1941)

APPENDIX

TABLE III - OBSERVED EQUIVALENT WIDTHS

HD 135485

λ	W (mÅ)	-log W/λ	Ident.
4922.1			He I
4900.4			S II
4859.6			Hβ
42.4			
15.6			S II
4804.9			Ti II
4788.1			N II
83.2			
49.6			
16.2	44	5.03	S II
13.1	303	4.15	He I
04.2	19	5.39	N II
4703.7	35	5.13	
4663.0	50	4.97	Al II
53.4	23	5.31	
47.0			
43.1	51	4.96	N II
38.9	27	5.24	Si III/O II
30.6	68	4.83	N II
29.3	32	5.16	Fe II
21.4	88	4.72	N II/Fe III

HD 135485 (cont.)

λ	W (mÅ)	-log W/λ	Ident.
4613.9	36	5.11	N II
07.1	39	5.07	N II
05.3			
4601.5	38	5.08	N II
4583.8	42	5.04	Fe II
80.0	14	5.52	
74.8	25	5.26	Si III
67.8	46	5.00	Si III
58.6	26	5.24	Fe II/(Cr II)
55.9	28	5.21	Fe II
52.5	84	4.73	Si III
49.5	83	4.74	Fe II
46.8			
41.8	23	5.29	Fe II
40.0			
4535.8	42	5.03	
29.2	54	4.92	Al III
25.0	39	5.06	S II
22.6	40	5.05	Fe II
20.2	35	5.11	Fe II
15.4	21	5.33	Fe II
4508.2	30	5.18	Fe II

HD 135485 (cont.)

λ	W (mÅ)	-log W/λ	Ident.
4491.5	35	5.11	Fe II/O II
81.2	355	4.10	Mg II
71.5	1360	3.52	He I
64.5	45	5.00	S II
63.6	54	4.92	S II
62.7			(Fe III)
54.2			
51.5	21	5.33	Fe II
47.0	50	4.95	N II
37.6	166	4.43	He I
34.0	44	5.00	Mg II
32.4	33	5.13	S II
28.0	33	5.13	Mg II/N II
25.9			A II
19.7	29	5.18	Fe III
4416.8	44	5.00	Fe II/O II
4390.6	62	4.85	Mg II
88.0	1030	3.63	He I
85.4	20	5.34	Fe II
84.7	47	4.97	Mg II
82.3	21	5.32	Fe III
58.5			O II/(A II)

HD 135485 (cont.)

λ	W (mÅ)	-log W/λ	Ident.
4357.7			Fe II
51.8	39	5.05	Fe II
40.5			H γ
38.8			Fe II
4303.1			Fe II
4296.5			Fe II
94.3	27	5.20	S II
90.3			(N III)
82.8			S II/O II/(A II)
69.8	36	5.07	S II
67.1	319	4.13	C II
41.7	56	4.88	N II
37.0	50	4.93	N II
33.2	54	4.89	Fe II
30.9	32	5.12	S II
27.6	30	5.15	Al II/N II
24.7			
17.1	39	5.03	S II/(Cr II)
11.2			(Fe III)
4200.7			
4198.1			Si II
90.7			Si II

HD 135485 (cont.)

λ	W (mÅ)	-log W/λ	Ident.
4189.6	40	5.02	S II/O II/(A II)
82.3	25	5.22	
78.8	40	5.02	Fe II
76.1			N II
73.5	84	4.70	Fe II/N II
69.0	130	4.51	He I
64.8	54	4.89	(Fe III)
62.6	56	4.87	S II
53.1	46	4.96	S II
50.0			Al III
49.1			
45.0	36	5.06	S II
43.8	1020	3.61	He I
43.2			Fe II
32.8	37	5.05	O II
30.9	161	4.41	Si II
28.0	133	4.49	Si II
20.8	255	4.21	He I
16.9			
4101.7			H δ
4090.1			
76.8	46	4.95	Si II/N II

HD 135485 (cont.)

λ	W (mÅ)	-log W/λ	Ident.
4076.0	60	4.83	Fe II/C II
75.5	47	4.94	Si II
74.7	41	5.00	C II
67.0	28	5.16	Ni II
48.8			Fe II
46.8			Fe II
43.5	18	5.35	N II
41.3	40	5.00	N II
40.2			
36.7			
35.1	29	5.14	N II
32.8	35	5.06	S II
28.9	28	5.16	
26.2	1830	3.34	He I
16.2			
4009.3	990	3.61	He I
3998.7	32	5.10	S II
95.0	81	4.69	N II
93.6			S II
90.9	34	5.07	S II/Fe III
86.1			
70.0			H ε

HD 135485 (cont.)

λ	W (mÅ)	-log W/λ	Ident.
3968.5			Ca II
64.7	62	4.81	He I
55.8	37	5.03	N II
54.2	32	5.09	O II
52.4			
34.1			
33.7	228	4.24	Ca II
33.3			
31.6			
30.5			Fe II
27	579	3.83	He I
23.4	43	4.96	S II
21.9			
20.6	119	4.52	C II
18.9	108	4.56	C II
05.9			Fe II
03.6	16	5.39	
3900.7	37	5.02	Al II
3888.9			H ζ
76	88	4.64	C II
72	360	4.03	He I
67.5	246	4.20	He I

HD 135485 (cont.)

λ	W (mÅ)	-log W/λ	Ident.
3862.6	113	4.53	Si II
60.8			S II/Fe II
56.0	133	4.46	Si II
53.6	83	4.67	Si II
50.9	32	5.08	O II
48.2	63	4.79	Mg II
35.2			H_9
19.6	1530	3.40	He I
3806.6			Si III
3797.6			H_{10}
83.4			Fe II
70.5			H_{11}
61.3	14	5.43	Ti II
59.3	48		Ti II/Fe II
56.0			
50.0			H_{12}
36.9	29	5.11	Ca II
34.3			H_{13}
21.7			H_{14}
12.5			H_{15}
3704.4			H_{16}
3692.9			

HD 135485 (cont.)

λ	W (mÅ)	-log W/λ	Ident.
3641.4			Fe II/Ti II
3554.5			He I
3548.2			

HD 37058

λ	W (mÅ)	-log W/λ	Ident.
4922.0			He I
00.1	25	5.29	(S II)
4896.1	17	5.46	
79.0	17	5.46	
75.7	10	5.69	
71.5	8	5.79	
70.5	14	5.54	
61.3			Hβ
25.5	17	5.45	Fe II
21.0	17	5.45	Ti II
19.2	39	5.09	Cl II
4809.7	43	5.05	
4794.3	48	5.00	Cl II
79.5	13	5.57	N II
67.9	14	5.53	(Ti II)
38.2	20	5.37	C II/(Mn II)/Cl II
28.9	10	5.67	
27.9	12	5.59	(Mn II)
22.7	12	5.59	Ca II
22.2	12	5.59	
4713.1	182	4.41	He I

HD 37058 (cont.)

λ	W (mÅ)	-log W/λ	Ident.
4692.7	14	5.52	(La II)
80.5	12	5.59	(Ce II)
57.1	16	5.46	Fe II/Ti II
55.6	17	5.44	Ti II
50.8	17	5.44	O II
50.2	10	5.67	C III
49.2	34	5.14	O II
43.0	21	5.34	N II
38.7	20	5.36	O II
30.4	48	4.98	C II/N II
21.4	29	5.20	O II/Fe III/N II/(Cr II)
19.4	38	5.08	
13.8	23	5.30	N II/O II
07.1	41	5.05	N II
4601.5	34	5.13	Fe II/N II
4596.1	39	5.07	O II
88.0	10	5.66	Al II/A II/(P II)
83.7	21	5.34	Fe II
74.7	50	4.96	Si III
72.0	48	4.98	Ti II/Cl II
67.9	68	4.83	Si III
58.8	12	5.58	(Cr II)

HD 37058 (cont.)

λ	W (mÅ)	-log W/λ	Ident.
4555.5	27	5.23	Fe II/(O III)
52.6	97	4.67	Si III
49.6	84	4.73	Fe II/S II/Ti II
48.2	10	5.66	
43.4	24	5.28	
40.2	18	5.40	
33.8	32	5.15	Ti II
29.1	26	5.24	Al III
24.8			S II/Ti II
22.6	21	5.33	Fe II
4512.5	19	5.38	Al III
4481.2	196	4.36	Mg II
79.9	23	5.29	Al III
78.5			S III
71.6	1200	3.57	He I
47.0	52	4.93	N II
43.7	21	5.33	Ti II
37.6	91	4.69	He I
34.0	19	5.37	Mg II
31.0	49	4.96	Fe III/(A II)/S II
19.6	48	4.97	Fe III
16.9	31	5.15	Fe II/O II

HD 37058 (cont.)

λ	W (mÅ)	-log W/λ	Ident.
4414.8			O II
4411.2	46	4.98	
4395.8	69	4.81	Fe III/Ti II/O II
92.0	24	5.26	S II/(Ne II)
87.9	727	3.78	He I
82.6	33	5.12	Fe III
72.5	86	4.71	Fe II/III/C II/(A II)
71.3	30	5.16	A II/C II
52.6	40 (6% H)	5.04	(Cr II)/Fe III
40.5			H γ
37.9			Ti II
17.2	30	5.16	O II
10.3	32	5.13	Fe III
04.5	31	5.14	(Fe III)
4300.0	34	5.10	Ti II
4296.6	34	5.10	Fe II
90.3	21	5.31	Ti II
86.1	24	5.25	Fe II/Fe III
85.6	30	5.16	O II
84.0	12	5.55	
69.8	20	5.33	S II
67.1	250	4.23	C II

HD 37058 (cont.)

λ	W (mÅ)	-log W/λ	Ident.
4253.5	41	5.02	(Ce II)/Cl II/S III/O II
47.0	24	5.25	(Sc II)
41.8	32	5.12	N II
41.2	14	5.48	Cl II
36.9	33	5.11	N II
35.6	28	5.18	Cl II/Fe III
33.1	22	5.28	Fe II/(Cr II)
15.6	52	4.91	Ti III
07.4	22	5.28	Ti III
04.8	24	5.24	Ti III
4200.0	43	4.99	Ti III/Fe III
4189.7	20	5.32	A II/S II/O II
89.1	20	5.32	Al III/Fe III
76.1	21	5.30	N II/(Ce II)
74.2	14	5.47	Ti II/Fe III/S II
73.5	16	5.42	Fe II/N II/Ti II
69.0	50	4.92	He I
66.9	22	5.28	Fe III
64.7	52	4.90	Fe III
63.7	21	5.30	Ti II
62.8	12	5.54	S II/C III
53.2	26	5.20	Fe II/S II/O II

HD 37058 (cont.)

λ	W (mÅ)	-log W/λ	Ident.
4143.8	768	3.73	He I
39.3	30	5.14	Fe III
37.8	28	5.17	Fe III
30.9	50	4.92	Si II
28.0	57	4.86	Si II
20.9	290	4.15	He I/Fe III
19.1	39	5.02	O II
12.1	15 (6% H)	5.44	Fe II/O II
4101.7			H δ
4080.9	18	5.35	A II/O III
77.8	22	5.27	(Cr II/Sr II)
75.9	78	4.72	Fe II/O II/C II
74.5	42	4.99	C II
72.2	40	5.01	O II
70.9			(Cr II)/Ni II
69.7	51	4.90	O II
68.6	21	5.29	C III/(Ce II)/(Sc III)
53.0	20	5.31	A II/Fe III
43.4	18	5.35	N II
41.3	26	5.19	N II/O II
26.3	1160	3.54	He I
17.4			C II

HD 37058 (cont.)

λ	W (mÅ)	-log W/λ	Ident.
4009.3	414	3.99	He I
06.6			
05.6	22	5.26	Fe III
05.0	27	5.17	Fe III
4003.1			Fe III/Cr II)
3995.0	66	4.78	N II
70.1			HE
68.4			Ca II (H)
64.7			He I
55.8	29	5.13	N II
54.4	36	5.04	O II/Fe III
33.7			Ca II (K)
26.7	277	4.15	He I
24.8			(La II)
21.5	47	4.92	(La II)
20.7	107	4.56	C II
19.0	86	4.66	C II
17.8			S II
15.3	50	4.89	(Cr II)
13.5	24	5.21	Ti II
3900.4	33	5.07	Ti II/A II/Al II
3889.0			H ζ

HD 37058 (cont.)

λ	W (mÅ)	-log W/λ	Ident.
3880.6	22	5.25	C II
76	94	4.62	C II
72	293	4.12	He I
67.6	246	4.20	He I
62.6	39	5.00	Si II
60.8	57	4.83	S II/III/Cl II/Fe II
59.5			Al II
57.3	18	5.33	O II
56.0	66	4.77	Si II/(N II/O II)
53.7	27	5.15	Si II
51.0	52	4.87	S II/O II/Cl II
45.5	22	5.24	A II/Cl II/Fe III
35.4			H 9
19.7	780	3.69	He I
06.9			Fe II
3806.5			Si III
3797.9			H_{10}
91.3			Si III/O III
83.1			S II/Fe II
80.2			
70.5			H_{11}
61.3			Ti II

HD 37058 (cont.)

λ	W (mÅ)	-log W/λ	Ident.
3759.3			Ti II/Fe II
57.7			Ti II
50.1			H_{12}
41.6			Ti II/Fe II/O II
34.4			H_{13}
21.9			H_{14}
12.0			H_{15}
05.6			(Cl III)
04.9			He I
3703.9			H_{16}
3685.2	36	5.01	Ti II
82.8			Fe II
75.7			
52.0			He I
49.6			
34.3	74	4.69	He I
13.6	79	4.66	He I
03.8			Fe II/Fe III/(Cr II)
3600.9			Fe III
3587.3			He I
3586.1			Fe III
3504.9			Ti II

HD 37058 (cont.)

λ	W (mÅ)	-log W/λ	Ident.
3422.6			Ti II/(Cr II)
3383.7			Ti II
3372.7			Ti II/Ca III
68.0			(Cr II)/S II
61.1			Ti II/C II
54.6			He I
53.8			N III
49.4			Ti II/(Cr II)
49.0			Ti II
38.6			Fe III
23.1			Fe II
05.1			O II/Fe III
3302.2			Fe III
3266.9			Fe II/Fe III
61.6			Fe II/Ti II/(Cr II)
39.7			Ti II
39.0			Fe III
36.6			Ti II
3234.5			Ti II
3187.5			(Ne II)

HD 37129

λ	W (mÅ)	-log W/λ	Ident.
4861			H β
4716	30	5.20	Si III, S II
4713	310	4.18	He I
4575	19	5.38	Si III
4568	50	4.96	Si III
4553	81	4.75	Si III
4481	179	4.40	Mg II
4471	1315	3.53	He I
4438	93	4.68	He I
4388	787	3.75	He I
4340			H γ
4267	155	4.44	C II
4169	81	4.71	He I
4144	667	3.79	He I
4131	36	5.06	Si II
4128	41	5.00	Si II
4121	154	4.43	He I
4102			H δ
4026	1085	3.57	He I
4009	406	4.00	He I
3995	29	5.14	N II

HD 37129 (cont.)

λ	W (mÅ)	-log W/λ	Ident.
3970			HE
3968			Ca II (H)
3965			He I
3933			Ca II (K)
3927	340	4.06	He I
3921	68	4.76	C II
3919	55	4.85	C II
3889			H ζ
3867	168	4.36	He I
3862	30	5.11	Si II
3856	53	4.86	Si II/(N II/O II)
3835			H_9
3819	761	3.70	He I
3806			Si III
3798-04			H_{10-16}
3705			He I
3634	178	4.31	He I
3614	58	4.79	He I

FIGURE 8α
BALMER PROFILES

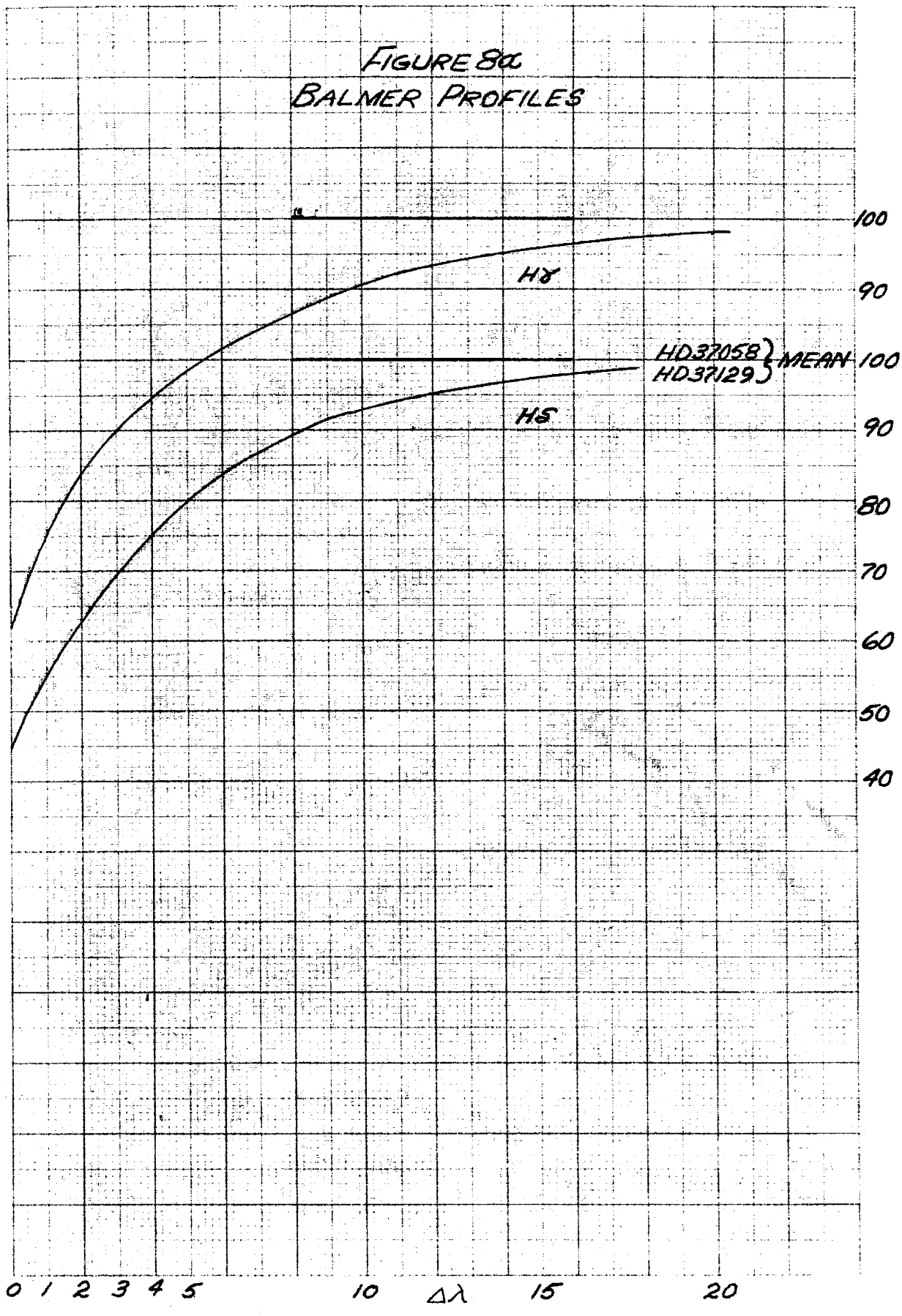

FIGURE 86
BALMER PROFILES

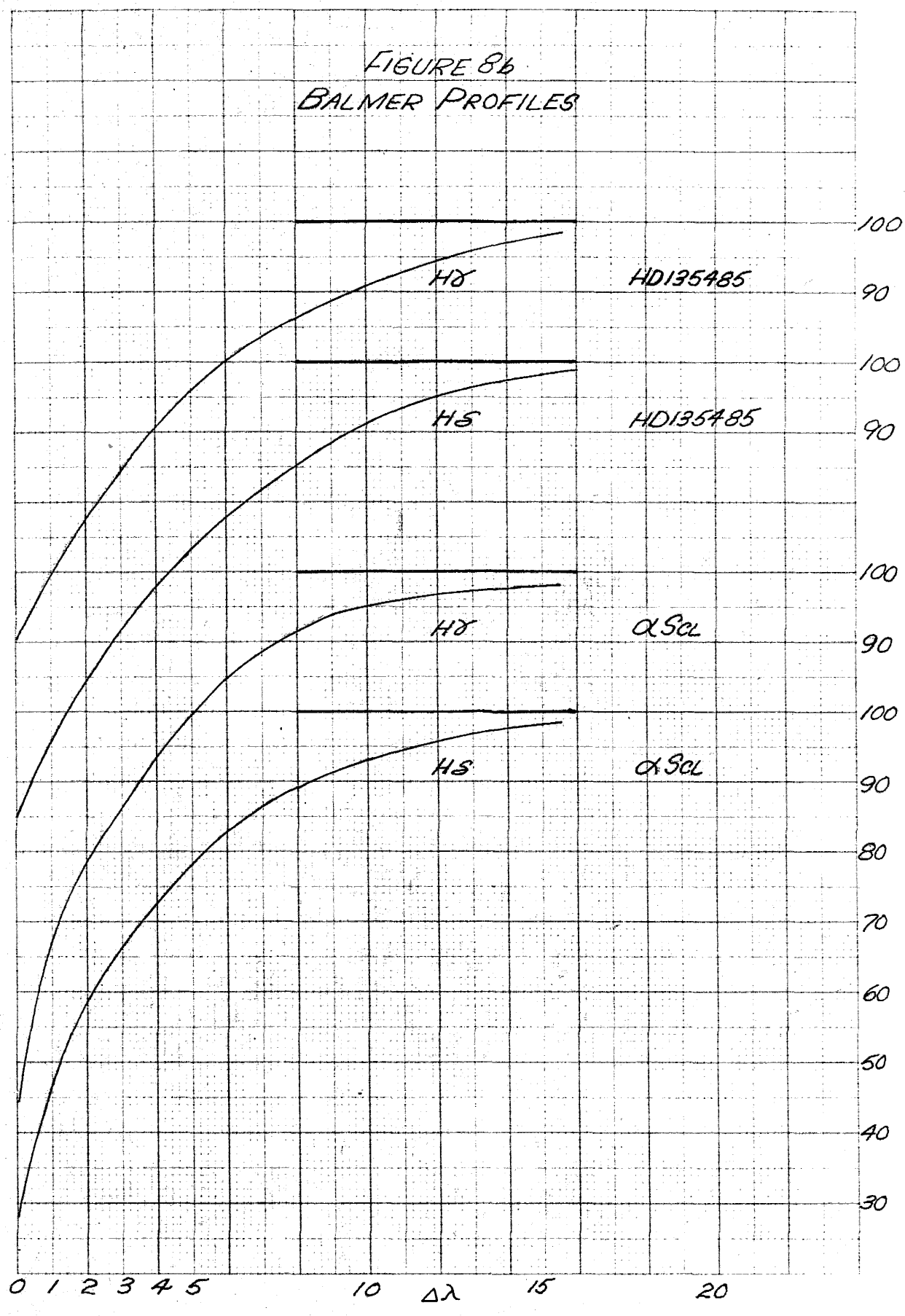

TABLE IV

RADIAL INTEGRALS

Ion	Array	σ^2
C II	3p - 4s	1.82
	3d - 4f	.63
	$2s2p(^3P^o)3d' - 4f'$	.51
N II	$2p(^2P)3s - 3p$	4.89
	$2p(^2P)3p - 3d$	1.18
	$2p(^2P)3p - 4s$	2.46
	$2p(^2P)3d - 4f$	.61
	$2s2p^2(^4P)3p' - 3d'$	1.21
O II	$2p^2(^3P)3s - 3p$	4.28
	$2p^2(^3P)3p - 3d$	1.22
	$2p^2(^3P)3d - 4f$	.66
	$2p^2(^1D)3p' - 3d'$	1.16
Mg II	3d - 4f	.66
	3d - 5p	.0073
	4p - 5d	.082
	4p - 6s	.41

Ion	Array	σ^2
Al III	4p - 4d	1.92
Si II	3d - 4f	.625
Si III	$3s(^2S)4s$ - 4p	6.20
S II	$3p^2(^3P)4s$ - 4p	6.15
	$3p^2(^3P)4p$ - 4d	1.25
	$3p^2(^3P)4p$ - 5s	2.70
	$3p^2(^1D)4s'$ - 4p'	6.15
	$3p^2(^1D)4p'$ - 4d'	1.39
Ca II	4s - 4p	4.28
	4p - 5s	2.36

TABLE V

ABSOLUTE LINE STRENGTHS

C II

Array	Mult	log S(M)	χ	J	λ	log S
3p - 4s	$^2P^o - {}^2S$	1.04	16.26	3/2-1/2	3920.68	0.86
				1/2-1/2	3918.98	0.56
3d - 4f	$^2D - {}^2F^o$	2.12	17.97	5/2-7/2	4267.27	1.88
				3/2-5/2	4267.02	1.72
3d′- 4f′	$^4F^o - {}^4G$	2.44	24.17	9/2-11/2	3876.19	1.96
				7/2-9/2	3876.41	1.85
				5/2-7/2	3876.67	1.72
				3/2-5/2	3876.05	1.60
				9/2-9/2	3880.59	0.80
	$^4D^o - {}^4F$	2.28	24.27	5/2-7/2	4074.53	1.67
				7/2-9/2	4076.00	1.83
	$^2D^o - {}^2F$	1.98	24.50	5/2-7/2	4411.52	1.74
				3/2-5/2	4411.20	1.58

C II (cont.)

Array	Mult	log S(M)	χ	J	λ	log S
	$^4P^o - {}^4D$	2.11	24.55	1/2-3/2	4371.59	1.03
				3/2-5/2	4372.49	1.43
	$^2F^o - {}^4G$	—	24.68	7/2-9/2	4630.52	—

N II

Array	Mult	log S(M)	χ	J	λ	log S
3s - 3p	$^3P^o$ - ^3P	1.64	18.39	2-1	4643.09	0.78
				2-2	4630.54	1.26
				1-0	4621.39	0.69
				1-1	4613.87	0.56
				0-1	4607.15	0.69
				1-2	4601.48	0.78
	$^3P^o$ - ^1D	—	18.39	1-2	3955.85	—
	$^1P^o$ - ^1D	1.39	18.42	1-2	3995.00	1.39
3p - 3d	^1P - $^1D^o$	1.42	20.32	1-2	4447.03	1.42
	^1P - $^1P^o$	0.95	20.32	1-1	3919.00	0.95
3p - 4s	^3P - $^3P^o$	1.34	21.07	2-1	3856.07	0.48
	^1D - $^1P^o$	1.09	21.51	2-1	4227.75	1.09
3d - 4f	$^3F^o$ - ^3F	1.33	23.03	2-2	4076.83	0.65
	$^3F^o$ - ^3G	2.39	23.03	3-4	4043.54	1.89
				4-5	4041.32	2.00
				2-3	4035.09	1.77

N II (cont.)

Array	Mult	log S(M)	χ	J	λ	log S
	$^3D^o - {}^3D$	1.33	23.14	2-2	4173.51	0.69
	$^3D^o - {}^1F$	—	23.14	2-3	4241.79	—
	$^3D^o - {}^3F$	2.23	23.14	3-4	4241.79	1.86
				1-2	4236.93	1.53
				2-3	4237.05	1.70
	$^3P^o - {}^3D$	2.06	23.32	1-1	4427.97	0.98
	$^1F^o - {}^3G$	—	23.37	3-4	4552.54	—
3p′- 3d′	$^5D^o - {}^5D$	1.65	27.60	2-1	4704.33	0.49
				2-2	4702.57	0.35

Ion	Array	Mult	log S(M)	χ	J	λ	log S	log S(IC)
O II	3s - 3p	$^4P - {}^4D^o$	1.93	22.88	1/2-1/2	4650.84		0.86
					1/2-3/2	4638.85	0.85	0.88
					5/2-7/2	4649.14		1.53
		$^4P - {}^4P^o$		22.88	1/2-3/2	4317.14		0.80
		$^2P - {}^2D^o$	1.63	23.32	1/2-3/2	4416.98	1.15	1.16
		$^2P - {}^2P^o$	1.41	23.32	1/2-1/2	3954.37	0.76	0.75
	3p - 3d	$^4D^o - {}^4D$	1.56	25.54	3/2-1/2	3856.16	0.26	-0.25
					3/2-3/2	3851.04	0.46	0.44
		$^4D^o - {}^4F$		25.54	5/2-7/2	4072.16		1.71
					1/2-3/2	4069.64		1.33
					3/2-5/2	4069.90		1.53

Ion	Array	Mult	log S(M)	χ	J	λ	log S	log S(IC)
O II		$^4D^o - {}^2F$	—	25.54	5/2-5/2	3857.18	—	-0.10
					7/2-7/2	3851.47	—	-0.30
		$^4P^o - {}^4D$		25.73	5/2-7/2	4119.22	—	1.62
		$^4P^o - {}^4P$	1.56	25.73	3/2-5/2	4153.30	0.74	1.19
					1/2-3/2	4132.81	0.70	1.05
		$^4P^o - {}^2F$	—	25.73	5/2-5/2	4112.03	—	0.37
		$^2D^o - {}^2D$		26.14	5/2-5/2	4395.95		1.03
	$3p' - 3d'$	$^2F^o - {}^2G$	2.10	28.24	7/2-9/2	4189.79	1.85	
		$^2D^o - {}^2F$	1.81	28.39	3/2-5/2	4703.18	1.41	

Ion	Array	Mult	log S(M)	χ	J	λ	log S	log S(IC)
O II	3d - 4f	$^4F - {}^4F^o$	1.49	28.56	5/2-5/2	4041.31	0.66	
		$^4F - {}^2F^o$	—	28.56	5/2-5/2	4035.09	—	
		$^2F - {}^4F^o$	—	28.74	5/2-7/2	4285.70	—	
		$^2P - {}^2D^o$	1.92	28.82	3/2-5/2	4491.25	1.70	
		$^2D - {}^4F^o$	—	28.94	5/2-5/2	4621.28	—	
					5/2-7/2	4613.67	—	
Mg II	3d - 4f	$^2D - {}^2F^o$	2.14	8.83	5/2-5/2	4481.33	0.60	
					5/2-7/2	4481.33	1.90	
					3/2-5/2	4481.13	1.74	
	3d - 5p	$^2D - {}^2P^o$	0.64	8.83	5/2-3/2	3848.24	0.42	
					3/2-1/2	3850.40	0.16	

Ion	Array	Mult	log S(M)	χ	J	λ	log S	log S(IC)
Mg II	4p - 6s	$^2P^o - {}^2S$	1.39	9.96	3/2-1/2	4433.99	1.21	
					1/2-1/2	4428.00	0.91	
	4p - 5d	$^2P^o - {}^2D$	1.69	9.96	3/2-3/2	4390.58	0.51	
					3/2-5/2	4390.58	1.47	
					1/2-3/2	4384.64	1.21	
Al III	4p - 4d	$^2P - {}^2D$	2.06	17.74	3/2-3/2	4528.91	0.88	
					3/2-5/2	4529.18	1.84	
					1/2-3/2	4512.54	1.54	

Ion	Array	Mult	log S(M)	χ	J	λ	log S	log S(IC)
Si II	$3s\,3p^2$	$^2D - {}^2P^o$	——	6.83	5/2-3/2	3856.02	——	
	$-3s^2 4p$				3/2-1/2	3862.59	——	
					3/2-3/2	3853.66	——	
	3d - 4f	$^2D - {}^2F^o$	2.12	9.80	5/2-5/2	4130.88	0.58	
					5/2-7/2	4130.88	1.88	
					3/2-5/2	4128.05	1.72	
Si III	4s - 4p	$^3S - {}^3P^o$	1.75	18.92	1-0	4574.78	0.80	
					1-1	4567.87	1.27	
					1-2	4552.65	1.49	

Ion	Array	Mult	log S(M)	χ	J	λ	log S	log S(IC)
S II	4s - 4p	$^4P - {}^4S^o$	1.39	13.59	5/2-3/2	4815.52	1.09	1.01
					3/2-3/2	4716.23	0.91	0.86
	4s'- 4p'	$^2D - {}^2P^o$	1.57	15.00	3/2-1/2	4552.38	1.09	1.09
					5/2-3/2	4524.95	1.35	1.35
	4p - 5s	$^4D^o - {}^4P$	1.73	15.84	7/2-5/2	4463.58	1.33	
					3/2-3/2	4432.41	0.76	
		$^4P^o - {}^4P$	1.51	16.04	3/2-1/2	4900.47	0.65	
	4p - 4d	$^4D^o - {}^4F$	2.32	15.84	7/2-7/2	4217.23	0.93	
					5/2-5/2	4189.71	1.04	
					7/2-9/2	4162.70	1.87	

Ion	Array	Mult	log S(M)	χ	J	λ	log S	log S(IC)
S II					5/2-7/2	4153.10	1.71	
					3/2-5/2	4145.10	1.52	
		$^4D^o - {}^4D$	1.57	15.84	7/2-7/2	4028.79	1.11	
					5/2-5/2	3990.94	0.81	
		$^4P^o - {}^4F$	—	16.04	5/2-5/2	4552.38	—	
		$^4P^o - {}^4D$	2.05	16.04	5/2-7/2	4294.43	1.65	
					3/2-3/2	4282.63	1.08	
					1/2-3/2	4269.76	0.97	
					3/2-5/2	4267.80	1.37	
		$^4P^o - {}^4P$	1.57	16.04	5/2-3/2	3860.64	0.75	
					3/2-5/2	3850.93	0.75	
		$^2D^o - {}^2F$	2.02	16.16	5/2-7/2	3933.29	1.78	
					3/2-5/2	3923.48	1.62	

Ion	Array	Mult	log S(M)	χ	J	λ	log S	log S(IC)
S II		$^4S^o - {}^4P$	1.70	16.18	3/2-5/2	4032.81	1.40	
					3/2-3/2	3998.79	1.22	
	4p'- 4d'	$^2F^o - {}^2F$	1.59	17.32	7/2-7/2	4189.71	1.33	
		$^2F^o - {}^2G$	2.18	17.32	7/2-7/2	4162.39	0.38	
					7/2-9/2	4162.70	1.93	
		$^2D^o - {}^2G$	—	17.37	5/2-7/2	4230.98	—	
Ca II	4s - 4p	$^2S - {}^2P^o$	1.41	0.00	1/2-1/2	3968.47	0.93	
					1/2-3/2	3933.66	1.23	
	4p - 5s	$^2P^o - {}^2S$	1.15	3.14	3/2-1/2	3736.90	0.97	